6-14-2013

A Graph theoretic approach to quantifying grey matter volume in neuroimaging

Ashley Zanca

R · I · T

A Graph Theoretic Approach to Quantifying Grey Matter Volume in Neuroimaging

By

Ashley T. Zanca

A Thesis Submitted in Partial Fulfillment of the
Requirements for the Degree of Master of Science in
Applied and Computational Mathematics

Department of Applied and Computational Mathematics
College of Science

Rochester Institute of Technology
Rochester, NY
June 14, 2013

Rochester Institute of Technology

School of Mathematical Sciences

Applied & Computational Mathematics Program

Master's Thesis

Applicant's Name: Ashley Zanca

Thesis Title: A Graph Theoretic Approach to Quantifying Grey Matter Volume in Neuroimaging

Proposed Defense Date: 6/14/2013

Advisor's name: Dr. Nathan Cahill

Committee Member 1: Dr. Linwei Wang

Committee Member 2: Dr Darren Narayan

Graduate Program Director: Dr. Tamas Wiandt

A Graph Theoretic Approach to Quantifying Grey Matter Volume in Neuroimaging

Ashley Zanca
Master of Science Thesis
Department of Applied and Computational Mathematics
Rochester Institute of Technology
Rochester, NY 14623,USA
June, 2013

Abstract

Brain atrophy occurs as a symptom of many diseases. The software package, Statistical Parametric Mapping (SPM) is one of the most respected and commonly used tools in the neuroimaging community for quantifying the amount of grey matter (GM) in the brain based on magnetic resonance (MR) images. One aspect of quantifying GM volume is to identify, or segment, regions of the brain image corresponding to grey matter. A recent trend in the field of image segmentation is to model an image as a graph composed of vertices and edges, and then to "cut" the graph into subgraphs corresponding to different segments. In this thesis, we incorporate image segmentation algorithms based on graph-cuts into a GM volume estimation system, and then we compare the GM volume estimates with those achieved via SPM. To aid in this comparison, we use 20 T1-weighted normal brain MR images simulated using BrainWeb[1] [2]. We obtained results verifying the graph-cuts technique better approximated the GM volumes by halving the error resulting from SPM preprocessing.

A Graph Theoretic Approach to Quantifying Grey Matter Volume in Neuroimaging

Ashley Zanca

Department of Applied and Computational Mathematics

Rochester Institute of Technology

Rochester, NY 14623,USA

June, 2013

Dedication

I dedicate my research to my parents. From whom I have learned the true meanings of tenacity, curiosity, strength, and scholarship.

Table of Contents

Extended Abstract

Brain atrophy occurs as a symptom of many diseases. The start of this thesis will review the various software packages and procedures used to quantify these symptoms. Symptoms involving grey matter (GM) expansion, white matter (WM) contraction, cerebral spinal fluid (CSF) distribution differences, brain function “job reassignment” are a few of the symptoms in the various diseases shared in Chapter 1. In this thesis and its connected research, we chose to focus on GM volume changes in brains.

The software package, Statistical Parametric Mapping (SPM) is one of the most respected and commonly used tools in the neuroimaging community for quantifying the amount of grey matter (GM) in the brain based on magnetic resonance (MR) images. Chapter 2 shares details of the voxel-based morphometry (VBM) process used in SPM. The stages detailed in this chapter include: spatial normalization, segmentation, modulation, and smoothing.

One aspect of quantifying GM volume is to identify, or segment, regions of the brain image corresponding to great matter. A recent trend in the field of image segmentation is to model an image as a graph composed of vertices and edges, and then to "cut" the graph into subgraphs corresponding to different segments. Chapter 3 dives into the fundamentals and algorithms of graph theoretic approaches in imaging, specifically segmentation. In this thesis, we incorporate image segmentation algorithms based on graph-cuts into a GM volume estimation system, and then we compare the GM volume estimates with those achieved via SPM. To aid in this comparison, we use 20 T1-weighted normal brain MR images simulated using BrainWeb[1] [2]. We obtained results verifying the graph-cuts technique better approximated the GM volumes by halving the error resulting from SPM preprocessing. The motivation behind this work as well as important software packages, containing BrainWeb, SPM, BrainSuite, etc. are included in Chapter 4. Chapter 4 also includes the algorithms behind the important methods used to complete the study.

Throughout this study, results were perfected. A few of these preliminary results along with corresponding qualitative and quantitative reflections are included in Chapter 5. Ultimately, the thesis concludes with graphs, figures, tables, as well as summaries of results, discussions, and future work in chapters 5 and 6. We found that MRI scans are particularly sensitive to data collection (machines, peripherals, and processing)[3], [4]. With SPM as a more common procedure for processing we found positive potential in further research and application of graph theoretic approaches. While GM volume estimations are imprecise, the relative error percentages of 1.6% and 8.4% for graph cuts and SPM procedures respectively. Demonstrating a more desirable procedure, graph cuts, to continue to expand research on.

Chapter 1

Introduction

For years the human brain has been an organ to discover, with a vast design to be understood. We will review the recent research that has attempted to quantify the structural brain changes associated with a plethora of disabilities, hyper-abilities, and developmental processes. The brain changes we will explore specifically involve grey matter volume changes. Our work will contribute to the uncertainty surrounding the relationship between the structural and functional changes in the brain. The research representing the correlations between grey matter volume and these conditions have been found in many ways across numerous studies, demonstrating a broad range of results. We will also examine the methods, algorithms, and processes

used to determine brain atrophy using structural magnetic resonance imaging (MRI) scans.

1.1 Diseases and Brain Atrophy

MRI scans can be used to determine a variety of structural brain changes. The brain develops and adapts over time; adaptations are the focus of many scientists, neurologists, and psychologists as they pertain to the human developmental phases, injuries, and environmental and natural influences. In this section, we will review studies that focus on structural brain changes in specific diseases, including narcolepsy with cataplexy, schizophrenia, type 1 diabetes mellitus, and other conditions.

1.1.1 Narcolepsy with Cataplexy

Narcolepsy with cataplexy is a sleep disorder where patents' brains cannot regulate their sleep-wake cycle and have sudden weakness in muscles. A major side effect of narcolepsy with cataplexy is the loss of hypocretin-(orexin-) producing neurons in the brain. Many studies involving sleep disorders have found structural brain changes. Schaer et al. [5] compared the subcortical and regional cortical volumes in high-resolution T1-weighted MRI images of twelve patients with narcolepsy and cataplexy with those of twelve healthy controls. They also compared whole-brain characteristics including cortical thickness and gyrification. These subcortical and regional cortical volumes were calculated using published algorithms included in the FreeSurfer package.[6] Schaer et al. observed a decrease in cortical volume in the left paracentral lobule and an increase in cortical volume in the left caudal part of the middle frontal gyrus in the patients with a diagnosis of narcolepsy with cataplexy as compared to the 'healthy patients' or controls. While the control group was matched for age and gender, it was small, so it is possible that alternate conditions such as drug dependency, alcohol consumption,

family medical history, hydration, etc. may the results. Fortunately, Schaer et al. suggested that future studies with larger sample groups to be used to distinguish the patterns that lie between narcolepsy and other non-hypocretin-deficient hypersomnia disorders. Schaer et al. [5] demonstrates the influence of the condition of narcolepsy with cataplexy on grey matter (GM) volume and revealed a noticeable change in other regions of the brain as well. However, as explained in Peelle et al.[7] the lack of consistency between age-related changes of grey matter volume may be influenced by a small sample size, or it may also be influenced by the choice of methods used (for classification, segmentation, normalization, etc.), various statistical models, or an uneven sample distribution. Ultimately, Peelle et al.[7] stresses the value of verifying methodological approaches, inferences, and assumptions used in a study.

1.1.2 Schizophrenia

Cobia et al.[8] studies the correlation between brain changes and schizophrenic behavior (or the relationship between neuroanatomical and cognitive measures) over a two year period. While the size of their subject group (thirty-eight schizophrenics and twenty-seven controls) is not large, they were able to detect significant brain atrophy over time in the middle frontal, superior temporal, and middle temporal gyri of individuals with schizophrenia. Unfortunately, they were unable to define a relationship between the progression of cortical thinning (in the frontal and temporal regions) in schizophrenia and the individual's clinical (neuropsychological) symptoms. This may be due to a lack of correlation or the results of an inaccurate/incomplete detecting method. They recommend further investigation in additional regions of the cerebrum. Kim et al.[9] had a different perspective when researching schizophrenia. As with any condition, different cycles of brain atrophy can be an effect of the stage of the condition. This pattern is displayed with GM loss, in the prefrontal and temporal cortices, advancing throughout the duration

of schizophrenia. Kim et al. focused on measuring cortical thickness between first-episode and chronic schizophrenia, and found no significant global cortical thickness differences between first-episode schizophrenia patients and controls or chronic schizophrenia patients and controls. Regional cortical thinning was detected in the temporal lobe (TL) of those patients with first-episode schizophrenia and further thinning in the prefrontal cortex (PF) was found in the chronic schizophrenic patients. Thickness was determined by calculating the difference between related vertices of a reconstructed inner and outer cortical surface.[7][5] It is important to note that these results vary from each other but both support results from previous research[10][11]. This may be a matter of detection and processing algorithms used, or other contributors of brain atrophy involved, or defining criteria (such as duration of illness) for first-episode schizophrenia.

1.1.3 Alzheimer ’s Disease

Many scenarios leading to changes in the brain are correlated with neurological and psychiatric dysfunctions. Alzheimer’s disease (AD) can be classified as one of these as it is a disease amongst schizophrenia and developmental disorders. These minor changes are at a level of such intricacy that AD remains as one of the unsolved diseases constantly being researched. Mechelli et al.[12] analyze the approaches, specifically with voxel based morphometry (VBM), for detection of brain atrophy. Mahanand et al.[13] presented a unique way to classify brain regions associated with this disease. This state of the art approach called, Self-adaptive Resource Allocation Network (SRAN), is used in conjunction with VBM and SPM software, all of which will be discussed in further detail in the upcoming sections. GM volume is one of the many forms of brain atrophy studied with Alzheimer’s disease; for years, researchers have been investigating everything between whole-brain atrophy and white matter changes to

cerebral spinal fluid changes and fluctuations in the left caudate nucleus.

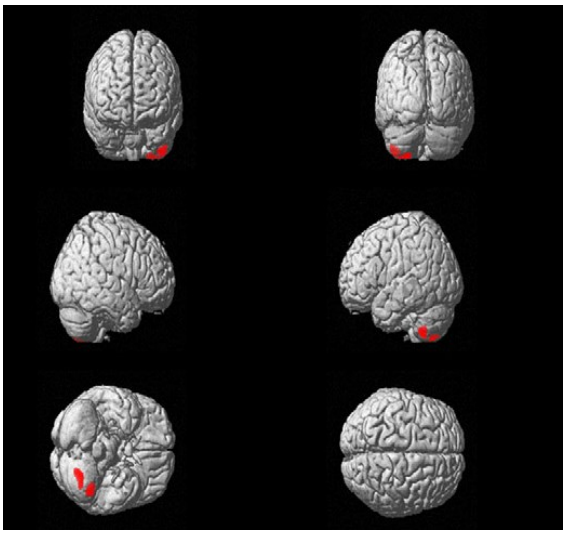

Figure 1.[14] Dynamic GM volume loss demonstrated in regions colored red on three dimensional rendered views in blind subjects with respect to partial blind subjects

1.1.4 Type 1 Diabetes Mellitus (T1DM)

Type 1 diabetes mellitus (T1DM), is a form of diabetes mellitus that is insulin dependent, as the body's autoimmune system destroys insulin producing cells. As we can see, the study of dynamic correlations involving severity of some condition (demonstrated in Figure 1), stage of the condition, passing time, and specific exposures is appealing in brain atrophy studies. Whole brain atrophy in addition to region specific atrophy has been analyzed as well. Results finding no significant whole brain changes were detected between T1DM patients and non-diabetic controls, over a two year longitudinal study working with seventy-five T1DM patients and twenty-five non-diabetic siblings, conducted by Perantie et al.[15] However, grey matter volume loss was detected along the dynamic spectrum of

glucose exposure (specifically at the glycemic extremes); those with more hyperglycemia tended to have a greater loss in whole brain GM volume. Perantie et al. improved the detection of deviation in developmental stages for these individuals, providing an improved basis for treatment and understanding. Chen et al. [16] points out the many damages type II diabetes can cause in a patient's nervous system, cardiovascular system, senses, kidneys, etc. and were proactive in investigating the structural changes of the brain. Their results show evidence of structural grey and white matter volume changes- most of which were in the right temporal lobe.

Given that a human brain undergoes functional and structural changes over time, Kalpouzos et al.[17] established a profile of human brain neurobiological changes with normal aging. This study involves the investigations of MR, PET, and ^{13}FDG-PET (PET images tracking Fludeoxyglucose throughout the body) scans using primarily voxel based methodology. Results from this study[17], affirms that brain changes follow genetic programs and cellular developmental processes as well as relate with memory abilities. Changes in the hippocampal volume follow an organic pattern expressing growth through childhood, stability through adulthood, and decay after 60s. Studies involving patients after the age of sixty or before the age of twenty should consider the possible influences these age defining transformations can make.

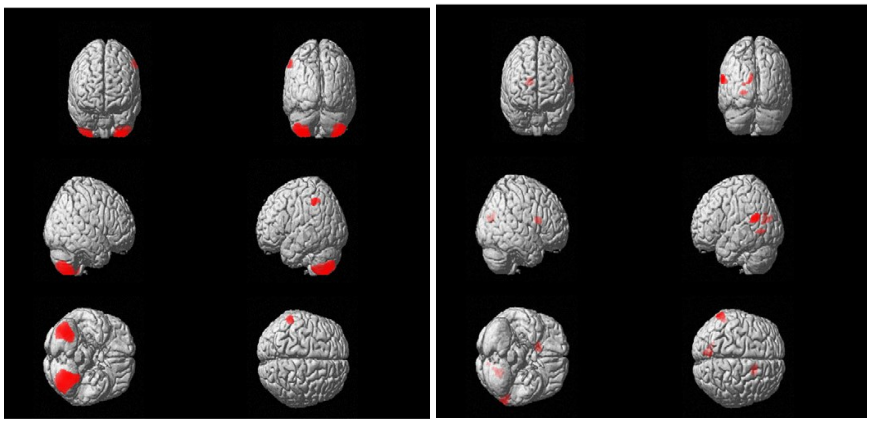

Figure 2.[14] Regions of GM volume loss demonstrated in red on three dimensional rendered views in: (left) blind subjects with respect to controls; (right) partially bind subject with respect to controls.

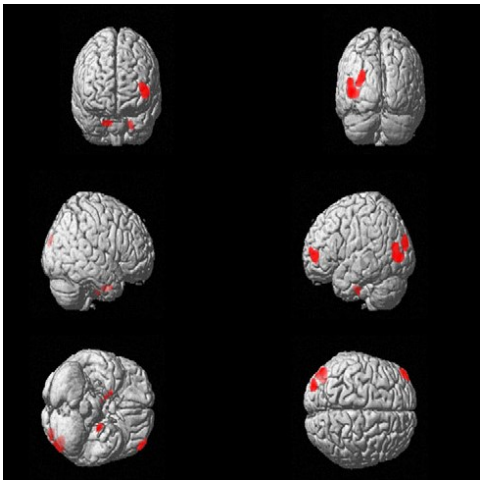

Figure 3.[14] GM volume increase in blind subjects when compared to controls are demonstrated in regions colored red.

1.1.5 Blindness

The Nuclear Magnetic Resonance (NMR) Research Center conducted a study[14] that investigates high resolution structural MR images of fifteen healthy sighted, thirteen blind, and six partially blind subjects and examines brain atrophy in relation to vision impairment. This dynamic analysis allows results to define relationships at multiple levels. The analysis used a Diffeomorphic Anatomic Registration Through Exponentiated Lie algebra algorithm (DARTEL) toolbox in

SPM8[14] and a VBM approach when concluding that subjects with vision loss at an early age have less visual input, which significantly decreases grey matter (GM) volume in the cerebellum with the vision impaired subjects with respect to the controls (Figure 2). Similar to that of the patients with narcolepsy and other brain altering conditions, Modi et al.[14] note an increase in GM volume in supplementary regions of the brain for those blind patients as compared to the controls (Figure 3). We may consider this work comparable to any other sensory loss; blind patients have to compensate for their loss of vision, stimulating learning and growth, which possibly causes the development and reorganization of other areas of the brain.

1.1.6 Lesions

Neuroimaging studies have demonstrated changes in MR-based measurements of brain volumes of subjects influenced by many psychological, physiological, and physical conditions. Most of these studies compare the brains of patients with abnormalities to those in a control group. While we will be working specifically with grey matter volume atrophy, it is important to notice the "trigger effects" of outside influences. "Trigger effects" are also considered secondary ramifications (or side effects) that must be considered in the decisions and conclusions of a study. It has been found that white matter (WM) lesions can affect the accuracy of brain volume calculations depending on the assessment method(s) being used.[18][3] Battaglini et al.[18] used five healthy subjects in combination with six lesion masks (created from six patients with different lesions) to create thirty "artificial" images. Each of the five original subjects' MR images was reconstructed to contain a lesion of each of the six lesion mask lengths. Brain tissue classification and segmentation are critical in many studies involving the calculation of volume estimation. Upon measuring GM volume in MR images, image classification and segmentation were two stages where WM lesions became a source of

error. Previous work has indicated that refilling the WM lesions with an intensity closely associated with that of the nearby healthy WM may resolve erroneous GM volume measurements.[18] A gain when working with lesions is that there is a physical and quantifiable interference in the image, whereas psychological disorders may not be detected or clinically followed-up on (based on the patient's lifestyle and habits). Studies often choose to work with subjects that have an absence of bystanding conditions to prevent otherwise - influenced data. However, (1) these bystanding conditions may not be detectable and (2) The absence of these bystanding conditions can be considered as a condition of its own (defined as, all subjects having similar habits/ lifestyles where they do not have the bystanding conditions). Hence, this strict avoidance of bystanding conditions can alter the data as well.

1.1.7 Prosopagnosia

The loss of face recognition, or prosopagnosia, is a condition acquired from brain trauma or strictly developmental. When a study is performed regarding a symptom and brain atrophy[17][19] the results can often apply to other studies or provide insight to a general body of diseases. When a study correlates a disease with brain atrophy[5][9][15] the results provide different information, of which is specific to a group of individuals interested in the disease. A study that was conducted by Garrido et al.[20] demonstrates a correlation between GM loss in regionally specific areas of the brain relating to face and object detection and recognition. Garrido et al. examined the whole brains of seventeen developmental prosopagnosia patients and eighteen controls using MRI scans and behavioral tests. Their work implemented several widely used tools including VBM and SPM5[21] (as automated procedures determining the GM volume), the Montreal Neurological Institute (MNI) template (used for registration)[22] and DARTEL [23](for inter-subject registration).[20]

These tools are commonly used in the medical imaging community and will be discussed further, in the “Tools” section.

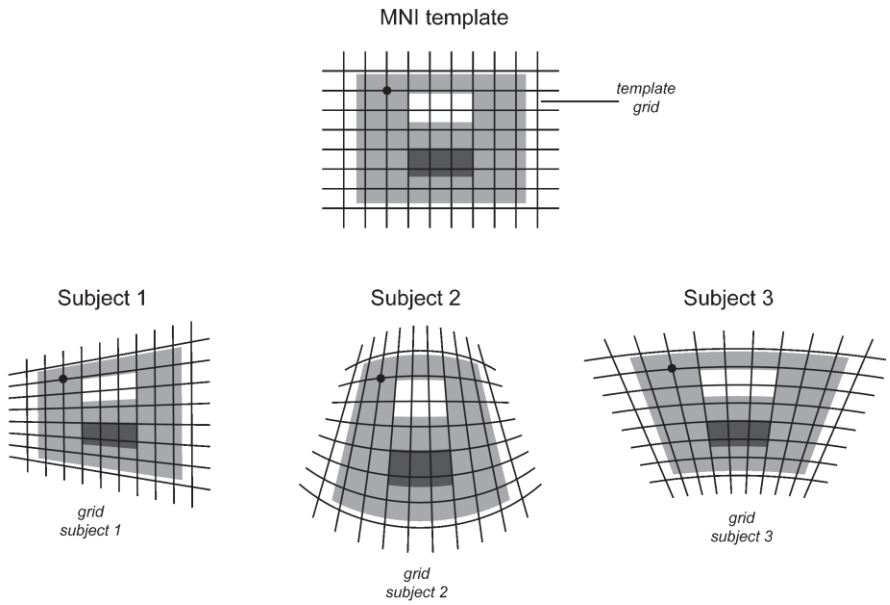

Figure 4.[24] The MNI template is used to normalize all brains to a standard space. The above MNI grid and the grid of subjects 1-3, consider represents the brains of three subjects and the MNI template, as labeled. Notice, the grids are not identical and grid points reference the same location in all subjects and template.

1.1.8 Social Anxiety Disorder (SAD) and Dehydration

Recently, MRI scans of individuals (thirteen undedicated adults with a diagnosis of generalized social anxiety disorder (SAD) and thirteen matched healthy controls) were examined to detect the cortical thickness of grey matter in people with SAD.[25] The MRI images were analyzed using FreeSurfer Version 4.5[6] [25, p. 301] to approximate the subcortical volumes and cortical thickness of the subjects. Exploration detected no regions in the SAD patients were thicker than those of the controls.[25] One of the main limitations with this work is the quantity of subjects participating in the research, which may have contributed to their results. Streitbürger et al.[19] completed another recent study investigating the volumes of GM,

WM, and cerebrospinal fluid (CSF) and found significant GM volume decrease due to dehydration and WM volume increase during 'hyperhydration'. Segmentation procedures used the FreeSurfer image analysis suite similar to the research completed by Schaer et al.[5], Syal et al.[25], and Winkler et al. [26]

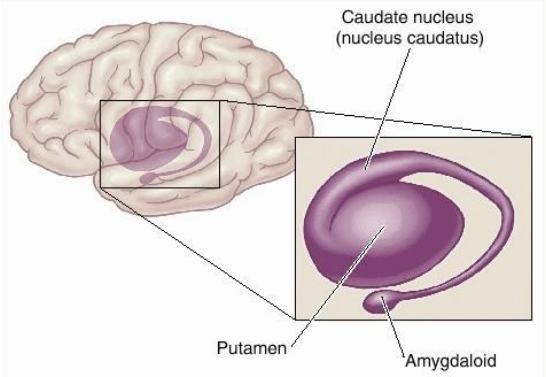

Figure 5. [27] Caudate Nuceus in lateral view of left side of brain

The exploration of the dynamic changes across different hydration state images indicated affected areas such as the left caudate nucleus (for perspective see Figure 5), a region also noted to be aligned with brain atrophy from Alzheimer's disease (AD) [19]. Many of these investigations conclude a correlation between a condition and brain atrophy. What may be more beneficial is exploring the relationship between symptoms and brain changes, as these symptoms may be applied to several different conditions allowing for more uses out of the data and results.

1.2 Problem Solving: Tools, Methods, & Parameters

While tools exist for studying brain atrophy, recent work[28][29][30] investigates how certain tools affect results. Peelle et al.[7] gave attention to the idea that different algorithms, methods, and programs may provide altering results. Peelle et al. studied the volume changes relating to age progression. Results show that there exists a depending factor between brain region volume changes and the methods or

statistical procedures used. This work was completed on a relatively large subject group (420 adults) with a normal distribution of age (between 18-77 years). [7] The study confirmed a volume decline in all areas of the brain when relating to age progression. In the search for optimal results, studies have considered,

(1) Their choice of programs[7] or software selection
(2) To conduct method alterations- such as fusing brain data to gather correlations between regions [31] or combining preexisting algorithms[32]
(3) To optimize parameter input- such as slice thickness for multispectral tissue classification (MTC) of brain tissues[33].

In the following sections we will discuss several tools for method alteration and choice of parameters.

1.2.1 Voxel-based Morphometry (VBM)

Voxel-based morphometry (VBM) is a neuroimaging tool commonly used to measure brain volumetry. VBM rids most significant differences between subjects' brain anatomy by registering each brain to the same stereotactic space (normalization in Figure 6) and then segmenting the substance of focus. The images are smoothed (such that each voxel is an average of itself and its neighbors), and the resulting image volumes are compared by relating every voxel. A summary of the VBM process can be seen in Figure 6.

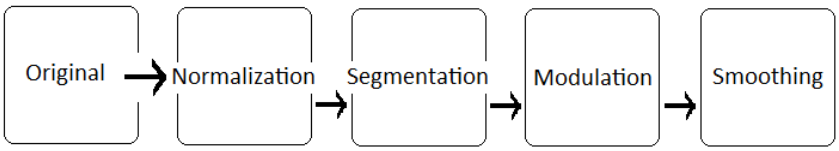

Figure 6. The process of VBM in simplest terms. Starting with an original image, after undergoing the process of VBM, the output displays regions where tissue types differ from groups correlated to a specific parameter

1.2.2 DARTEL

DARTEL[23] is another common program applied on MRI brain images to perform inter-subject registration research or realignment of small inner structures. DARTEL is an algorithm for diffeomorphic image registration. Registration is a way of transforming various datasets to one coordinate system; approximating a correlation between points in one image to the points in another image. In Figure 7 [34] we can see differences in brain sizes between the subjects in the right panel. We notice in the left panel that the ability to correlate individual reference points between subjects is clearer due to the smooth and correlated mapping results of the DARTEL process. Among the studies utilizing DARTEL algorithms in their analysis procedures is the research completed by Chen et al.[16] at PLA General Hospital, Beijing, China. As stated earlier, their results show evidence of type II diabetes relating to structural grey and white matter volume changes, most of which were in the right temporal lobe.[16]

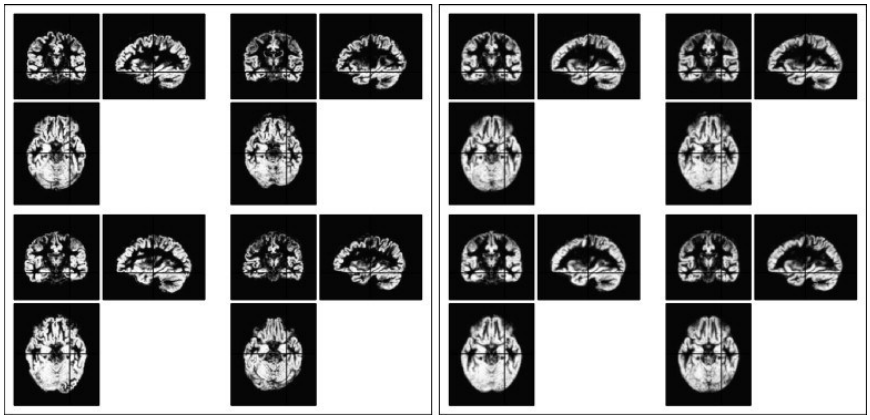

Figure 7. [34]The left panel displays four subjects: 18 year old female, 79 year old female, 67 year old male, 17 year old male, (from upper left moving clockwise) The Right panel demonstrates the same after normalization and warping using DARTEL.

DARTEL was used in the preprocessing step of VBM and all structural image data was processed using Statistical Parametric

Mapping 8 (SPM8) with MATLAB 7.6 [16] similar to the work of many others including Modi et al. [14] , Peelle et al.[7], and using SPM5 Garrido et al.[20] and Frings et al. [35]. While Chen et al. recognized a few limitations in their work and discussed ideas for future efforts, one notable limitation, which applies to other studies is, using other registration methods to increase the accuracy of inter-subject volume changing values.

1.2.3 Variations on Segmentation

1.2.4.1. Expectations Maximization Segmentation (EMS) & Histogram-Based Segmentation Algorithm (HBSA)

Many research applications, including volumetry, have segmentation as a critical step in image processing[3]. This critical step in analysis (most commonly executed for results as described in Figure 8) produces a need for segmentation techniques. Consequently, over the past ten years various methods have been formed to match the pace of development in neuroimaging for medical and research purposes. Valuable processes such as, the Bayesian principle, integrating prior knowledge into an existing method can lead to a more accurate algorithm for the task at hand. A comparative examination[3], conducted on the accuracy of MRI segmentation algorithms, suggests that SPM2 and Expectations Maximization Segmentation ((EMS) an open source code[36]) are both reliable methods to be used when working with partial volume correction (PVC) in MRI based studies. However, when there are no lesions in the brain to be corrected, the histogram-based segmentation algorithm (HBSA) produces preferable results for WM classification and EMS for GM classification.

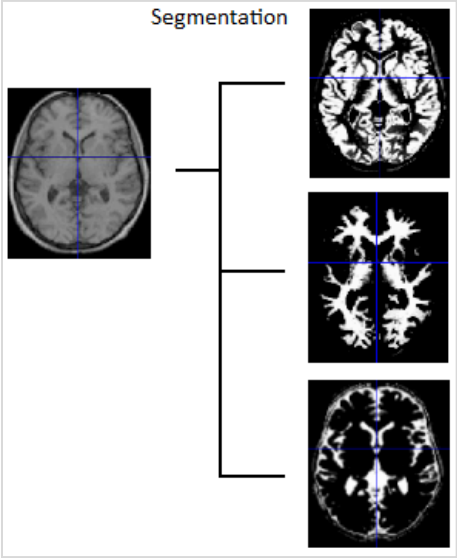

Figure 8. An example of segmentation of an original brain scan (left) partitioned it into GM, WM, and CSF (right; from top to bottom respectively).

1.2.4.2. Graph Theoretic Segmentation & Fully- Automated Segmentation

The inclusion of graph theory is one of the newest perspectives in the neuroimaging and brain networking research communities. Recent work of Liang et al.[37] presents a fully automated hemispheral segmentation algorithm and compares their results with those produced from commonly used software packages. Their algorithm uses Graph Cuts[38] techniques and was found to have significantly lower misclassification than the three packages it was tested against (BrainVisa, SurfRelax, and CLASP). This automated hemispheral segmentation algorithm worked with three spatial regions: left cerebral hemisphere (LCH), right cerebral hemisphere (RCH), and cerebellum and brainstem (CBB). Classification of these three regions is made after two main steps of boundary surface determination (1) between the cerebrum and CBB and (2) between the left and right

hemispheres. [37] However, the tissue segmentation our research will be working with contains problems of a dissimilar focus, as it involves segmentation into GM, WM, and CSF from MRI scans.

As with many other research scenarios, the quantity of promising approaches becomes problematic [3]. Three problems with approaches include:

1. Inconsistency between research results
2. A lack of adaptability due to a wealth of specificity within procedures
3. A supply of general results that is slow to aid further clinical analysis.

Zaidi et al.[3] focused their study on the influence of segmentation results on MRI-guided PVC and chose segmentation algorithms to compare for robustness. They critiqued the algorithms based on the reliability and availability (to the neuroimaging community). [3] This type of comparative analysis is becoming increasingly important in all studies, beyond PVC needs. Neuroimaging analysis has allowed early detection and tracking of many diseases.

1.2.4 A Variation of Classification - Self-daptive Resource Allocation Network

We have discussed the importance of validating methods in preparation for authenticating how the tools will be utilized. Great advancement and development of tools has come while employing structural MRIs. Some of the most recent and distinctive work includes: classification techniques using self-learning methods such as Self-adaptive Resource Allocation Network (SRAN) of Mahanand ‘s et al. work on Alzheimer’s disease.[13] Also, automated MRI volumetry tested by detecting specific patterns of brain atrophy in patients with frontotemporal lobar degeneration (FTLD). Specifically, Frings et al. worked with seven patients with semantic dementia

(semD), six with behavioral variant FTLD (byFTLD), four with progressive nonfluent aphasia (PNFA). The focus was on the correlation between ratios of changing volume in the temporal lobes (TL)and frontal lobe(FT) (what has been previously been declared as the primary grey matter regions for atrophy in FTLD).[35]

1.2.5 Parameters

These self-learning methods are only a few examples of the choices amongst tools that can be utilized. Another choice is in the parameters, an instance of this can be seen with the work of Winkler et al., where choosing the appropriate neuroimaging phenotype was the inspiration behind their work. The human brain with all its complexities has been questioned for years with cortical thickness, GM volume, and surface area as a few of the most looked at brain phenotypes. Winkler et al. utilized neuroimaging advancements to interrelate brain development, reorganization, functionality, and structure with inhabiting or habiting conditions. When identifying genes that influence the brain, their results suggest that surface area has a stronger correlation with GM volume than cortical thickness with GM volume. Also, surface area is of higher interest in genetic studies than thickness, followed by GM volume. Winkler et al. used MRI scans of 486 individuals from random strings of ancestry[26] and demonstrates an interesting complex amongst the decisions researchers make regarding choice of methods, subjects, phenotypes, and processes considered.

1.3 Unsolved problems

One unsolved problem revolves around the diagnosis of Alzheimer's disease. Investigations[12][13][39][40] have suggested that patients with AD have a significant amount of whole-brain atrophy. While some research has been completed on the creation and evaluation of automatic algorithms, there is a general consensus in the medical and

imaging sciences communities that automated methods are needed to supplement the manual procedures. Research groups such as Zhang et al.[28] examine automatic volume-based image registration algorithms[28], and others such as K. Chen et al.[40] create them. K. Chen et al. proposed an automatic method for computing brain volume that works with MRI images and uses an iterative principal component analysis (IPCA) which uses the voxel pairs from coregistered MRI images. Amongst the several other previously mentioned techniques, digital subtraction is used for characterizing and contrasting MRI data from patients to gather whole-brain atrophy measurements. The method proposed by K. Chen et al. was found to detect down to 0.04% change in brain volume in an individual, thus, it is claimed to be both rigorous and precise with detecting small volume changes. Different than VBM, Dynamic Brain Mapping, or Regional Analysis of Volumes Examined in Normalized Space (RAVENS), IPCA needs no spatial normalization step, because it measures volume changes in the brain on a global scale where the 'control' values is each subject's individual baselines rather than a brain template space. The technique was used to detect brain volume changes over time with the potential to determine the progression in patients with AD. However, it can also be used to detect changes for normal aging individuals, [40] and potentially patients with schizophrenia, or brain trauma.

While we spoke about several tools that are commonly used, many research groups have used a combination of fully automatic tools with manual measurements to find their brain volume approximations. Among the mix of problem solving tools needed to detect for brain atrophy, we saw SIENA[41], SIENAX[4], FreeSurfer algorithms[6] , DARTEL[23], VBM[42] , SPM[21], RAVENS[43], and Dynamic Brain Mapping[44] each one relating to a stage of volume detection such as normalization, segmentation, boundary delineation, or volume detection, itself. Several recent studies have compared the rigor and

accuracy of specific procedures (and stages of the procedures) used when calculating GM volume [7][3][29][30], and overall found varying results based on the needs of the research (ie. smaller volume changes, longitudinal analysis, specific conditions being examined, etc.). Wang and Doddrell not only critiqued several preexisting methods of evaluating rate of change in brain atrophy, but created their own with a distinctive attribute to calculate voxels accurately along the tissue boundaries where potential partial volume problems occur. This unique feature is a fractional volume model. Manual tracing was averaged (two raters traced the regions two times each on separate occasions) to validate volume results[29], however, we must consider, the results are of merely four manual ratings. Thus, the lack of gold standards for comparing results creates a problem when trying to evaluate these tools made to analyze the estimation of brain atrophy. To evaluate the reliability of registration based methods and optimize their results, Sharma et al.[30] created simulations of brain deformations using BrainWeb images. The methods evaluated included SIENA, SIENA extended to a cross-sectional method (SIENAX), and brain edge motion analysis "Boundary Shift Integral" developed by Imaging of Dementia and Aging Lab., University of California, Davis (BSI-UCD). After comparing these methods on simulations it was determined that the quality of images may influence the difference in results. Two interesting finds include: Geometrical distortions lead to mean absolute errors (of 0.07%, 0.82%, and 1.68%)increasing in the order of SIENA, BSIUCD and SIENAX respectively and Interpolation artifacts were considered to have no notable effect [30].

The investigation of dynamic changes in the brain provides insight to the correlation between brain atrophy and the different stages of a condition (or incidents of severity). This form of research completed in many other projects including Schaer et al. [5] , Kim et al.[9], Cobia et al. [8], and Modi et al.[14] is important in the study of GM

volume. It reminds us of the abundance longitudinal analysis studies, which pursue brain volume and condition correlations, as well as the continuous need to interrelate all these conditions. Thus, while exploration ideally takes into account the various contributors to the data - the continuation of research only validates that there is always more to consider. Previous results have shown quantifiable evidence of GM volume changes:

(1) Between the 'unhealthy' MRI brain scans of those subjects with a condition progressing over time. (ie. the study computes the GM volume from the MRI brain scan of subject i, upon their k^{th} visit and compares it with the GM volume from the MRI brain scan of subject i, upon their $(k+1)^{th}$ visit, as described below)

$$Subject_i^k \ \ vs. \ \ Subject_i^{k+1} \ \ vs. \ \ Subject_i^{k+2} \ ...$$

(2) Between the 'unhealthy' brains of subjects with a condition and healthy brains of a control group. (ie. the study computes the GM volume from the MRI brain scan of subject i and compares it with that of the control)

$$Control \ \ vs. \ \ Subject_i^1$$

However, we are interested in comparing the healthy brains of a control group with the 'healthy' brains of subjects (later to be diagnosed with an abnormality). Thus, we may find correlations to support preventative detection rather than responsive discovery.

$$Control \ \ vs. \ Subject_i^1$$

Such that,

$$Subject_i^k \ has \ an \ abnormality \ detected, where \ k > 1$$

And

$$Subject_i^k \ has \ no \ abnormality \ detected, where \ k \leq 1$$

Chapter 2

Volume Detection

Grey matter volume can be calculated from a brain scan through VBM in SPM. The process goes as follows: fMRI scans are run through an SPM pipeline of which they can be considered standardized to work with. After modulation and spatial normalization, the images can be used to calculate GM volume. The volume can be considered as the sum of voxels in this image multiplied by the voxel volume[45]. We will look at this process in more detail.

2.1 Voxel-Based Morphometry

Voxel-based morphometry (VBM), uses voxel-wise comparisons to calculate the neuroanatomical differences, specifically volume of GM

concentration, between subjects at the local concentration level rather than the global level[42]. This is achieved though the following sequence of processes.

(1) Spatial normalization
(2) Tissue Segmentaiton
(3) Modulation
(4) Smoothing
(5) Statistical Analysis

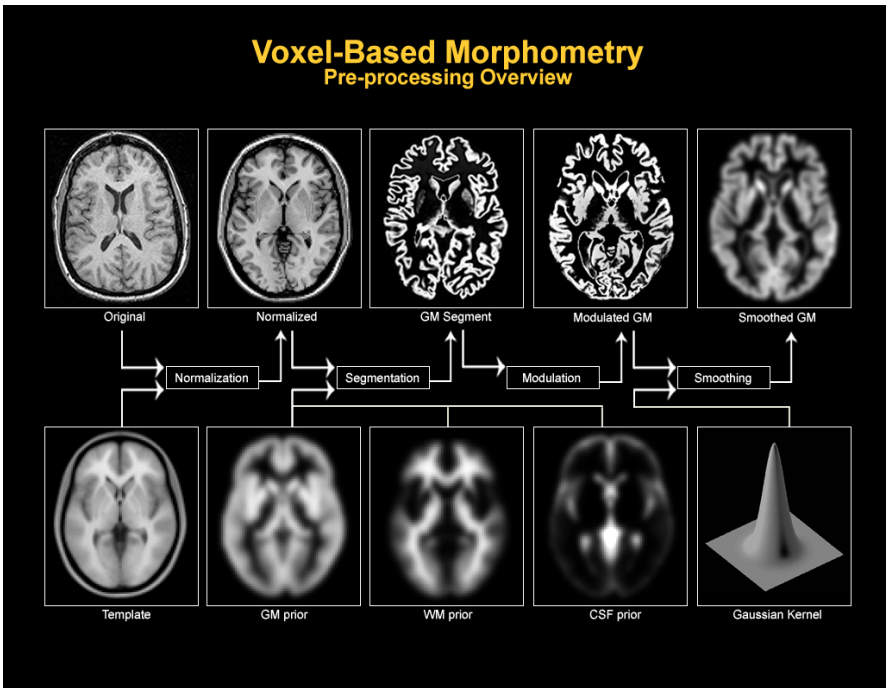

Figure 9. [46] See appendix I for larger display. This chart demonstrates the stages of VBM, starting from an original MR image to a smoothed image ready for statistical analysis.

2.1.1 Spatial Normalization

Spatial normalization of the images requires that each image be matched to a template, as shown in Figure 9[46]. Ideally the template consists of the average of a large quantity of MR images. The goal of spatial normalization is to minimize global brain shape or position

differences so that regional and more local differences can stand out. Each subjects' data is adjusted to match one common stereotactic space; thus, differences in individual brain size and shape will less likely be detected as GM volume differences.

As Ashburner states[42], the process of normalizing occurs by registering each image to the template while minimizing the residual sum of squared differences between them. Linear transformations such as rotation, scaling, translation, shearing help the original image to match the overall size and shape of the template, however, sometimes there are non-linear procedures including warping that is needed for the original image to match the template. These images should have a high resolution, of 1 or 1.5mm isotropic voxels, to assure accuracy in the later imaging processing stages.

2.1.2 Segmentation

With regards to GM, segmentation of the normalized image occurs by classifying every voxel in the original image as GM, WM or CSF by prior understanding of the probabilities of each (see Figure 9). MNI has a GM prior, WM prior, and CSF prior that provides the probability (between 0 and 1) at each voxel showing the intensity for each tissue type. The automated process within VBM compares the original image to the prior probability maps to define the probability of being of a certain tissue type. Recently, some studies[47] have been using the segmentation into a fourth and "other" classification preventing misclassification from lesions, etc.

The process where segmentation occurs before normalization is the defining aspect of optimized VBM[12]. While performing GM analysis, the differences being detected in the optimized VBM are only derived from GM data. Whereas, differences may occur before segmentation from global or various brain tissues, in the "normal" VBM process, influencing the statistical analysis of GM.

2.1.3 Modulation

As mentioned previously, non-linear spatial normalization may be needed in the earlier stages of VBM. These non-linear processes warp the brain volume data and can be corrected with modulation. Modulation is useful with studies seeking to identify changes regionally, consequently requiring the absolute volume be preserved.[42] The following equation is an example of corrected intensities. This means the intensity after spatial normalization, t_2 is set equal to the intensity before spatial normalization, t_1, multiplied by the local value in the deformation field. In this case, the local value is represented by the ratio of the volume before spatial normalization v_1 and the volume in the template v_2 .

$$t_2 = t_1(\frac{v_1}{v_2})$$

Non-modulated[12] images identify the differences in density of GM proportional to other tissue types, thus, the relative concentrations of GM structures in spatially normalized images. Modulated images relate the differences in calculated volume between GM volume and other tissue types, comparing the absolute volume of GM structures.

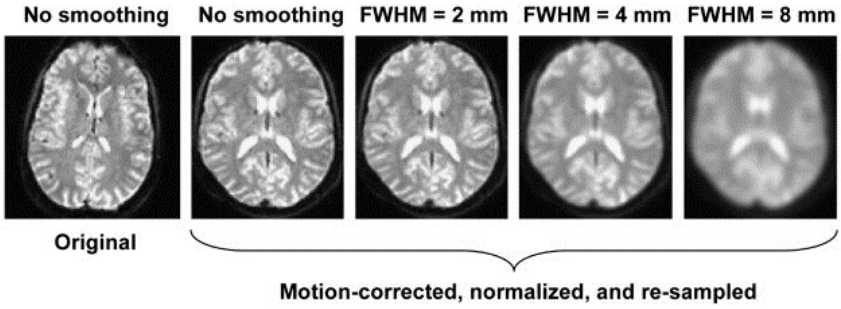

Figure 10. [48] The process of smoothing the image influences the data to become more normally distributed, however, the larger the kernel, the more spatial precision is lost. (From left to right) This figure demonstrates the original MR image before preprocessing and smoothing; after preprocessing (normalization, segmentation and modulation using SPM5) but still no smoothing; smoothing with a Gaussian kernel of three varying sizes (FWHM= 2mm, 4mm, 8mm) as labeled.

2.1.4 Smoothing

Smoothing is another stage for correction of inaccuracies from normalization. In simplest terms, for each voxel, a new value is generated as a function of the original value of that voxel and the values of the surrounding data. Notice in Figure 10. [48] The process of smoothing the image influences the data to become more normally distributed, however, the larger the kernel, the more spatial precision is lost. (From left to right) This figure demonstrates the original MR image before preprocessing and smoothing; after preprocessing (normalization, segmentation and modulation using SPM5) but still no smoothing; smoothing with a Gaussian kernel of three varying sizes (FWHM= 2mm, 4mm, 8mm) as labeled. At this stage of VBM each voxel becomes a weighted average of its surrounding voxels by convolving with an isotopic Gaussian kernel as demonstrated in Figure 9. The "surrounding voxels" is defined by the smoothing kernel which should be of a size comparable to the expected regional differences between groups of brains (usually between 8 and 14 mm)[42]. Often the form of referring to the Gaussian measurement is in terms of the full width half-maximum (FWHM), see Figure 11.

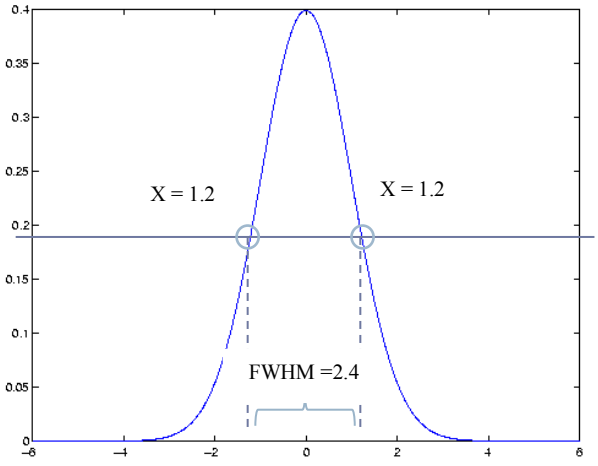

Figure 11. Here is a standard Gaussian with mean at zero and sigma of 1. The height is approximately 0.4 thus, half the height is approximately 0.2. The x-values (at the half-height) y=0.2 are x=-1.2 and x=1.2 meaning the width at y=0.2 is approximately 2.4. The FWHM= 2.4.

2.1.5 Statistical Analysis

The general linear model (GLM)[49], given below, is used to draw correlations between GM volume and specific effects within the study through a multitude of tests. The general linear model for a response variable x_{ij} at voxel j = 1, …, J with error ε_{ij} is:

$$x_{ij} = g_{i1}\beta_{1j} + g_{i2}\beta_{2j} + \cdots + g_{ik}\beta_{kj} + \varepsilon_{ij}$$

Where β_{1j} and K are unknown parameters for voxel j.

And the coefficients g_{ik} explain the conditions at which the observation/scan, *i,* was made (ie. these coefficients may be a covariate indicating cerebral blood flow (CBF), plasma prolactin levels, etc. or an integer value indicating a condition, subject, or drug).

The overlaying question in VBM analysis is, "Are the intensities different in the patient images versus the control images?" GLM provides the structure to complete group comparisons, identify regions of GM concentration relating to specific covariates, etc.[42]. These hypotheses can be tested with a simple t test. Output of Statistical Parametric Maps displays regions where tissue types differ between groups correlated with a specific parameter; specifically we are looking at the variation between volume calculations Figure 12. Results are often demonstrated:

- On 3D brain surface renders where coloring scales represent the most affected regions
- On a transparent display "glass brain" containing the voxels with most significant change
- On selected slices showing all voxels and the significant effected areas, often in color associated with t values

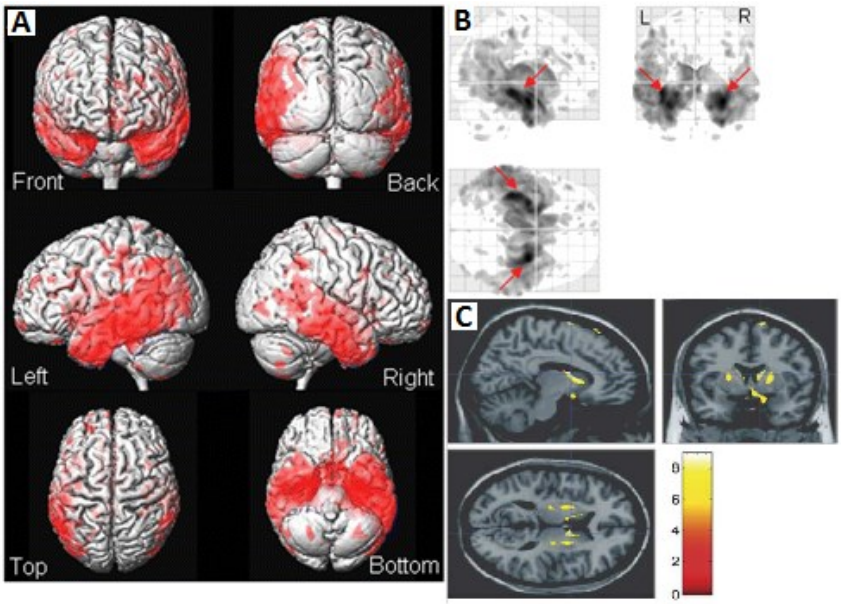

Figure 12. [50] Figure A shows six different views of a 3D render of the brain, with the voxels in red representing those with significantly reduced GM volume in subjects versus controls. Figure B shows the significant GM differences in a grayscale on the the sagittal, axial, and coronial views of a glass-brain. Figure C [51] demonstrates the sagittal, axial, and coronial views of the statistical parametric maps where Huntington's disease patients have lower GM intensity than controls. Specifically maximum intensity projection (MIP) is overlaid on the standard template. The color bar shows the z-score where the highest z value represents the greatest change.

There are many factors that may contribute to these volume differences, thus the intensity for voxel (V) can be thought of as a function of these contributors:

$$V = \beta_1(patient) + \beta_2(control) + \beta_3(covariates) + \beta_4(global\ vol.) + \varepsilon$$

$$\beta_3(covariates) = \beta_5(addiction) + \beta_6(age) + \beta_7(gender) + \cdots$$

Where β_3 are specific functions describing the association between the scan at voxel and the patient, control, covariates, etc. ε accounts for error in the computation.

Due to the large number of comparisons being performed during the statistical steps in VBM, it is important to correct for false positives Two common methods of preventing false positives are (1) the family-wise error (FWE) correction which controls the chance of false-positive across the entire volume and (2) the false discovery rate (FDR) correction which controls the proportion of false-positives among the effected voxels[50]. To correct for false positives, SPM uses gaussian random fields to determine the significance of these results[42].

2.2 Some Limitations of VBM

VBM has provided reliable information for a number of research studies. However, as with any method or process there are some weaknesses that may or may not be relevant to a study. We will now share several of the potential limitations of VBM:

i. Subject variance-
   Due to the fact VBM is searching for differences in the brain as corresponding to a specific feature. It is more difficult to pick up these changes between areas with high intersubject variance.
ii. Scanners-
   Images may display differences caused by the scanner rather than the subjects[42]. To prevent this, images should be collected on the same scanner with identical imaging parameters.
iii. Normalizing and segmentation-
   Image data may contain differences in data that is representing motion rather than brain atrophy consequently altering results of normalization and the tissue classifications. As this happens with any clinical study and is based on human

error, one of the biggest things researches can do is try to minimize and ideally eliminate this motion.

iv. Atypical brains-

Brains with different structures or features not present in the template[12] may be classified as an incorrect tissue type. Before further advancement on warp methods that model these pathologies, some solutions include integrating a fouth class for segmentation[47], "masking out" the abnormality[12], or smoothing the deformation fields to minimize displacement.

v. Data distribution-

Analysis through SPM uses parametric statistical analysis, assuming the data is normally distributed[42][12]; the data, however, may not be normally distributed. Thus, one solution for the assurance of accuracy can occur through nonparametric statistical analysis.

While the above are several potential limitations of VBM it is important to initially measure the right object (ie. That our variables are accurately defined). For instance, if we are seeking the GM volume difference, we want to be confident that we have identified the grey matter effectively. This discussion suggests the inclusion of an evaluation of the utilized segmentation method.

2.3 More Segmentation

Segmentation models can require that each voxel contain one of three tissue classifications. Because a voxel may contain more than one tissue type, Ashburner et al.[42] suggested it may be modeled incorrectly- this is common for the voxels between white matter and ventricles. In particular, many central grey matter structures are inaccurately classified due to their intensities closely representing those of WM.

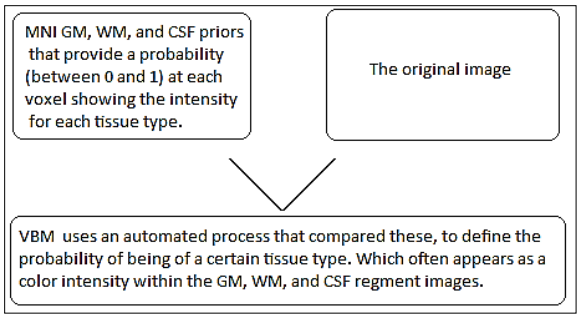

Figure 13. A conceptual display of segmentation in VBM, commonly used.

Segmentation of an image into its respective components happens by joining knowledge of the spatial distribution of different tissue types encoded in Bayesian priors[12] (Figure 13 is the original image after spatial normalization in a Bayesian framework[42]) with the voxel intensity distributions of each tissue type [12] (Figure 13 Figure 13is the MNI probability intensity priors). The VBM segmentation step also includes a nonuniformity correction[42] phase to compensate for smooth image intensity variations.

2.4 Evaluation

Ashburner et al. [42] evaluated the segmentation algorithm utilized with VBM. They used several simulated images of the same brain created by the BrainWeb simulator[1], similar to Sharma et al.[30]. Each of these images was classified (into GM, WM, and other) individually and in a multispectral manner, with three levels of nonuniformity (intensity variation), and both with and without sensitivity correction. Due to the fact these images were simulated, results of segmentation could be compared with the "true" GM, WM and other. Table 1 with Figure 14 presents the levels of accuracy calculated through k statistics between the values 0-1 (1 pertaining to most precise). We can see, in every case, the images including sensitivity correction produce more accurate segmentation results.

TABLE 1

	Single image			Multispectral			
	T1	T2	PD	T2/PD	T1/T2	T1/PD	T1/T2/PD
0%RF—uncorrected	0.95	0.90	0.90	0.93	0.94	0.96	0.94
0%RF—corrected	0.95	0.90	0.90	0.93	0.94	0.96	0.95
40%RF—uncorrected	0.92	0.88	0.79	0.90	0.93	0.95	0.94
40%RF—corrected	0.95	0.90	0.90	0.93	0.94	0.96	0.94
100%RF—uncorrected	0.85	0.85	0.67	0.87	0.92	0.94	0.93
100%RF—corrected	0.94	0.90	0.88	0.92	0.93	0.95	0.94

Table 1. [42] This table presents the different k statistics that were computed after segmentation. The k statistic represents the accuracy of the finding with respect to the "truth" (recall there exists a "true" GM segmentation because these images are simulated). The k statistic is directly proportional to the 'observed proportion of agreement (POA)' minus the 'expected POA' and inversely proportional to one minus the 'expected POA'[42]. The three levels of nonuniformity were: 0%RF (no intensity variation artifact), 40%RF (a typical amount of nonuniformity), 100%RF (a high and unusual amount of intensity variation) each of which were segmented with and without sensitivity correction. Figure 14 displays the simulated images and segmentation for the grey highlighted region of this table.

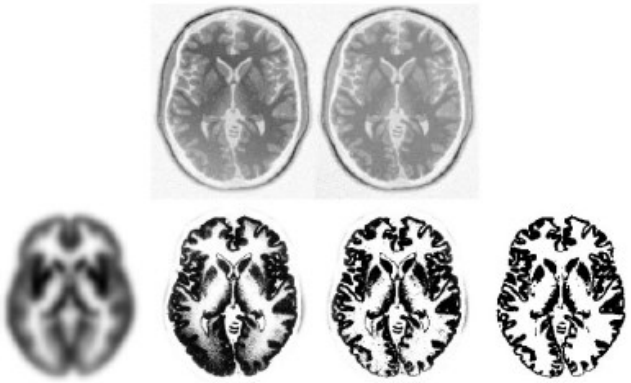

Figure 14. [42] The top row (from left to right) shows the original T1 weighted MR simulated BrainWeb[1] images: 100% nonuniformity and 100% nonuniformity corrected. The second row displays (from left to right): (1) the prior image used for segmentation of GM, (2) the GM segmented without nonuniformity correction, (3) the GM segmented with nonuniformity correction,and (4)the "true" distribution of GM.

Ashburner et al.[42] also conducted research on the relation between registration and segmentation by creating prior probability images that are translations of the true prior probability images. Using the same BrainWeb simulated images the scans were registered with these translated prior probability images. Results indicated how far a brain can deviate from the normal population of brains (the original and commonly used prior probability image) before losing robustness. A κ -statistic was calculated using the true GM and WM for the different translations,

$$\kappa = (p_o - p_e)/(1 - p_e)$$

Where the observed proportion of agreement, p_o, is the sum of the each category (K) number of agreements, f_{kk}, over the number of observations, N.

$$p_o = \sum_{k=1}^{K} f_{kk}/N$$

The expected proportion of agreement, p_e, is:

$$p_e = \sum_{k=1}^{K} r_k c_k / N^2$$

Where the number of voxels for the true partition is r_k, and the estimated partition is c_k , see Figure 15.

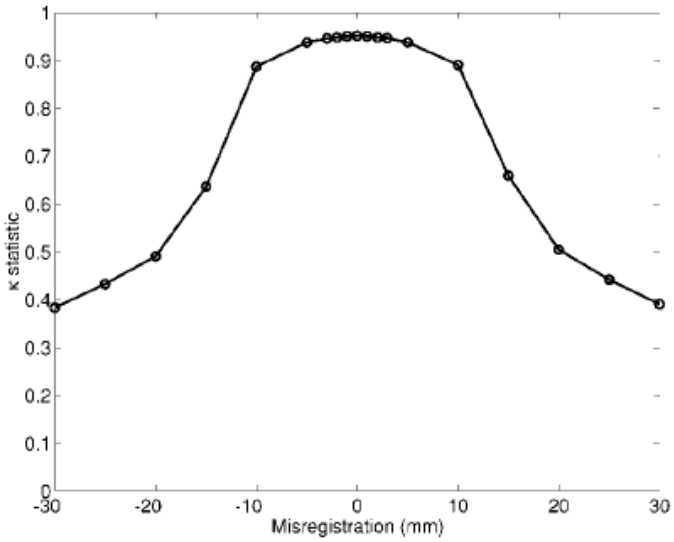

Figure 15.[42] displays the segmentation accuracy with respect to misregistration with a prior probability image. A k-statistic was calculated using the true GM and WM for the different translations,

Chapter 3

Segmentation

Segmentation is the stage of volume preprocessing we chose to focus on. This chapter goes into depth with the segmentation considerations and decisions made throughout our research.

3.1 Relation in Our Study

Due to the process of longitudinal work, the argument can be made, that the method(s) of calculating the volume need not matter as long as the method is consistently used with all data being compared. For instance, a young man may choose to have an assistant calculate his height using the 'standard $\delta -$ process' and compare it to the height of a control measurement. Suppose the assistant then measured the young man two years later using the same 'standard $\delta -$ process'.

Due to the consistency in any possible calculation errors the results would provide equivalent ratios. A bigger issue only occurs when the assistant utilizes a 'standard $\lambda-$process' in place of the 'standard $\delta-$process'. However, as scholars we have reasonable resistance with this thought and desire to use the ideal process, seeking both accuracy and preciseness. In any study, the methods, algorithms, and processes must fit the research accurately.

When analyzing the current practice and some of the limitations of VBM we chose to reevaluate, specifically, the process of segmentation. As one of the primary stages of analysis, segmentation divides the images into regions with similar attributes. While there are many forms of segmentation [37] [52], we looked to our interests (in graph cuts), strengths(in graph-based techniques), and mathematical background (in energy optimization) when choosing a spatially guided, energy based, graph-based, graph cut segmentation (see Figure 16). Spatially guided implies segmentation relies on the relationships between pixels; energy-based suggests the method intends to minimize cost functions; and graph-based denotes use of graph theoretic representations as the image form. We recognize segmentation as a powerful tool when quantifying brain volume, tissue definition, and anatomical design from MRI images. Segmentation is involved with a wide array of research topics such as brain development [53], [54], degeneration and diseases [15], [40], [44], [53, p. 1], neurological and psychological differences[31], [39], [51], IQ and memory processes[9][36][42][55], and much more. The need for effective segmentation has led to advancement and adjustments of the segmentation methods that exist today.

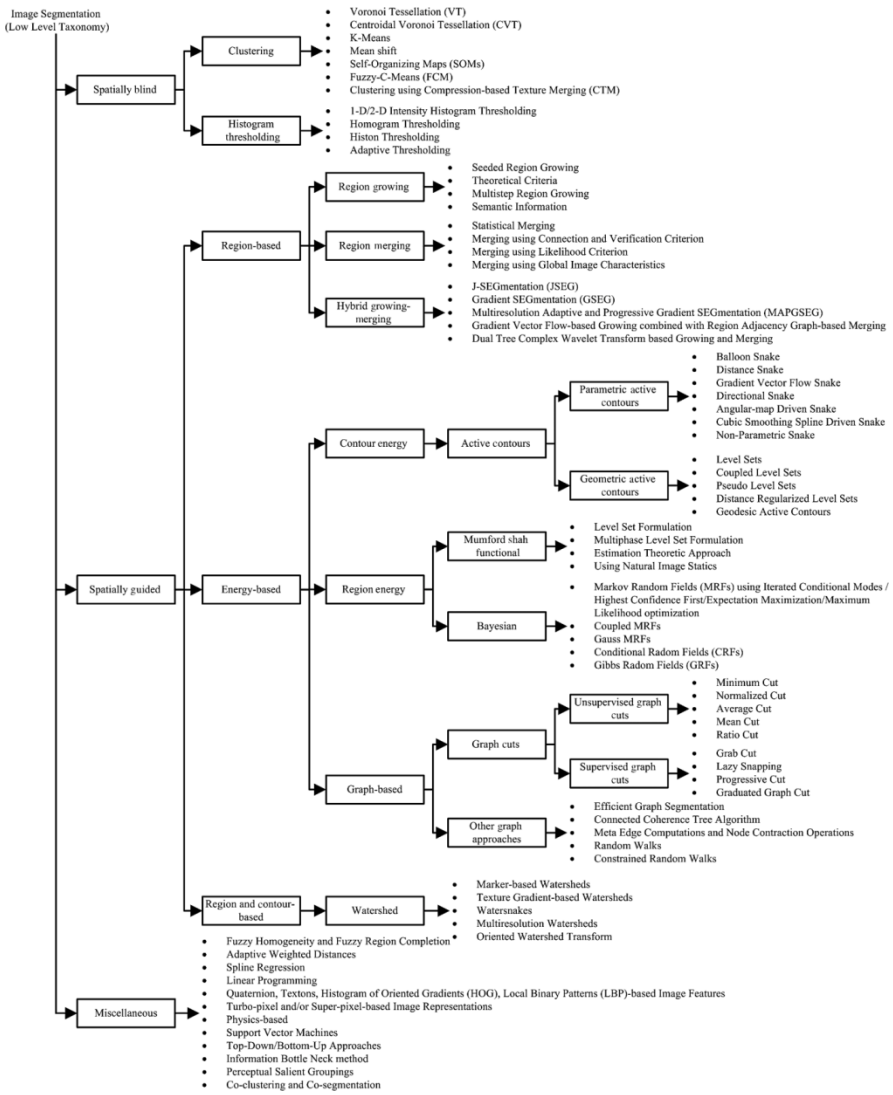

Figure 16. [52] See appendix II for larger display. This diagram displays a categorical hierarchy of segmentation techniques.

3.2 Graph Cut Segmentation

3.2.1 Fundamentals

Graph cut segmentation is an energy-based approach to image segmentation. Figure 17. [52] An example of an image in graph theoretic form. First, a cut is a partition of a graph into two disjoint subsets. An image can be represented as a graph $G = (V, E)$, where

nodes $v_i \in V$ correspond to individual pixels and edges $(v_i, v_j) \in E$ connect neighboring pixels v_i and v_j in graph $G = (V, E)$. Finally, each edge is assigned a weight w_{ij} based on the amount of similarity between the two neighboring elements.

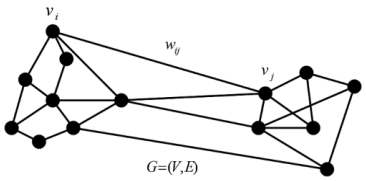

Figure 17. [52] An example of an image in graph theoretic form.

The objective of graph cuts segmentation is to partition the graph into subgraphs of related vertices[52]. This partition occurs with a cut or series of cuts. A cut, *C*, in graph theory is defined as a partition of V of graph $G = (V, E)$, specifically,

$$G(C) = (V, E - C).$$

Let us consider graph G in Figure 18. The left figure demonstrates a minimum cut, on the graph G. A minimum graph is a cut of minimum cardinality to create disjoint graphs. In graph G, the minimum cannot be 1 as there is no bridge. We can identify the two subgraphs as consisting of nodes {A, E, B} and {D, C} respectively. The middle figure demonstrates a maximum cut of five on graph H, with subsets consisting of {E, A, C} and {D, B}. A maximum cut is a cut of maximum cardinality to create disjoint graphs. In graph H, the maximum cut cannot be $|\boldsymbol{E}|$ (recall, $\boldsymbol{E}$ is the set of all edges) as H contains an odd cycle (H is not a bipartite graph). The right figure demonstrates an isolated node as a result of a min cut. However, the two subgraphs can be categorized with a 'better cut.' We can visually recognize these subgraphs as categories: 'tight nodes' and 'spacious

nodes'. The cost of the cut C, $|C|$, can be represented as the sum of its weighted edges,

$$|C| = \sum w_{ij}$$

$$\sum w_{ij} = w_{ED} + w_{BC} .$$

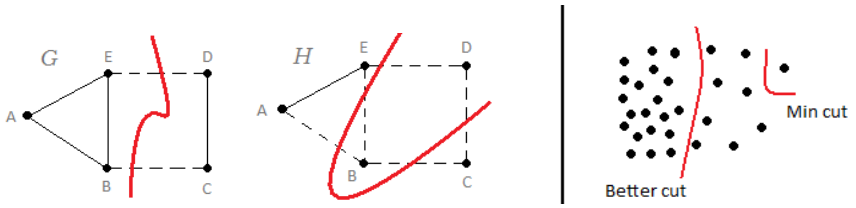

Figure 18. Similar to the idea stated in [56] The left figure demonstrates a minimum cut of two on the graph G. A minimum graph cut is one where there is no fewer edges that can be severed to create disjoint graphs. In graph G, the minimum cannot be 1 as there is no bridge. We can identify the two subgraphs as consisting of nodes {A, E, B} and {D, C} respectively. The middle figure demonstrates a maximum cut of five on graph H, with subsets consisting of {E, A, C} and {D, B}. A maximum cut is one where there is no cut that exists larger. In graph H, the maximum cut cannot be $|E|$ (recall, E is the set of all edges) as H contains an odd cycle (H is not a bipartite graph). The right figure demonstrates an isolated node as a result of a min cut. However, the two subgraphs can be categorized with a 'better cut.' We can visually recognize these categories as 'tight nodes' and 'spacious nodes'.

Wu et al.[57] was one of the first to utilize a graph theoretic approach in segmentation. The construction of an adjacency graph (see Figure 19) contains the weights of edges derived from a local derivative operator where strong edges were linked with small costs and weak edges were associated with large costs[52]. This algorithm produced a final segmentation with the minimum cut and least cost. While this would sometimes produce isolated nodes in the segmented graph such small partitions negatively impacted the accuracy of the method.

Consequently, a measure of disassociation between graph partitions, normalized cut (Ncut) measure, was computed[56] as follows:

$$Ncut(A,B) = \frac{|(A,B)|}{assoc(A,\ V)} + \frac{|(A,B)|}{assoc(B,V)}$$

Where $A \cup B = V$ and $assoc(A,\ V) = \sum_{u \in A, t \in V} w(u,t)$, in other words, the sum of weights (or similarity amongst verticies) from nodes in A to all nodes in the graph, V. We define $assoc(B,V)$ similarly and the numerators below:

$$|(A,B)| \ = \ cost\ of\ cut(A,B) = \sum_{u \in A, v \in B} w(u,v)$$

Thus, the isolated nodes will have a large Ncut value to be used in segmentation approaches[58]. This led to many more advancements

(1) reducing the computational work[59],

(2) broadening the application to region or pixel-based segmentation independent of size, shape and other varying contributors[60],

(3) developing an interactive algorithm relieving the unsupervised intense computational work as well as integrating better specificity in segmentation desires[61].

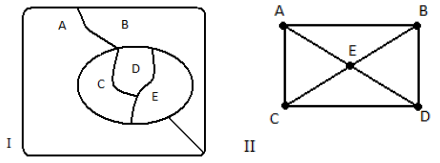

Figure 19. Diagram I demonstrates a segmented graph or an image with regions labeled A-E. Diagram II demonstrates an adjacency graph where nodes A-E correspond to the regions in diagram I and edges represent neighboring or "adjacent" regions. For instance, region A shares a border with regions B, C and E thus, in diagram II node A should have three edges (extending to nodes B, C, and E).

Recently, Boykov et al.[62] proposed two energy minimizing techniques, based on graph cuts, that are efficient with approximating label assignments to pixels. The multi-label optimization algorithms $\alpha - expansion$ and $\alpha - \beta - swap$ uniquely define simultaneous label changes based on expansion and swap moves, as opposed to the standard one pixel label change at a time.

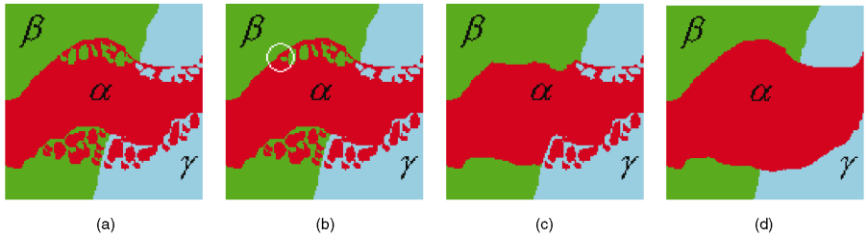

Figure 20. [62] An initial labeling (a) is demonstrated with three labels, $|L| = 3$, along with an example of a standard move (b) , $\alpha - \beta - swap$ (c) and $\alpha - expansion$ (d). Notice, for the standard move (b), a single pixel (marked by the circle) changes at a time, whereas (c) & (d) allow for simultaneous label changes.

First, consider $V_{p,q}$ as a distinct penalty (or relationship) between each pair of pixels $\{p, q\}$, let us define[62] $V_{p,q}$ as a *metric* on the space L if:

$$V_{p,q}(\alpha, \beta) = 0 \Leftrightarrow \alpha = \beta, (1)$$

$$V_{p,q}(\alpha, \beta) = V_{p,q}(\beta, \alpha) \geq 0, (2)$$

$$V_{p,q}(\alpha, \beta) \leq V_{p,q}(\alpha, \gamma) + V_{p,q}(\gamma, \beta), \ (3)$$

for any labels $\alpha, \beta, \gamma \in L$ and *semi-metric* if $V_{p,q}$ satisfies only (2) and(3). $\alpha - \beta - swap$ is to be used with *semi-metric* $V_{p,q}$ and $\alpha - expansion$ with *metric* $V_{p,q}$.[1]

[1] Further explanation on these concepts can be found in Boykov et al. [62].

Thus, for our research we will be using $\alpha - expansion$ which can be better understood as:

> Given a label α and an initial partition **P**, a move from **P** to **P'** (where **P'** is a new partition) is an $\alpha - expansion$ if $P_\alpha \subset P'_\alpha$ and $P_l \subset P'_l$ for any label $\neq \alpha$. This process is described in more detail in section 3.2.2.

Whereas, for our reference, $\alpha - \beta - swap$ can be thought of as:

> Given a pair of labels α, β and an initial partition **P**, a move from **P** to **P'** (where **P'** is a new partition) is $\alpha - \beta - swap$ if $P_l \subset P'_l$ for any label $\neq \alpha, \beta$. (ie. some pixels labeled α in **P** will now be labeled β in **P'**, and some labeled β in **P** will now be labeled α in **P'**).

3.2.2 Algorithms

The $\alpha - expansion$ algorithm, as described in Boykov et al.[62][63], [64], [65], [66], is as follows:

Algorithm: $\alpha - expansion$

---

1. Start with an arbitrary labeling f
2. Set success := 0
3. For each label $\alpha \in L$
   - 3.1. Find $\hat{f} = \arg\min E(f')$ among f' within one $\alpha - expansion$ of f
   - 3.2. If $E(\hat{f}) < E(f)$, set $f := \hat{f}$ and success := 1
4. If success = 1 goto 2
5. Return f

Recall what we have discussed this far about graph cuts. Step 3.1 in the above algorithm is the primary difference between the $\alpha -$

$expansion$ and $\alpha - \beta - swap$. This $\alpha - expansion$ method was called in the graph cuts segmentation script that proceeded as follows:

Algorithm: Graph Cuts Segmentation

---

1. Make list of label values: select label values for each image
2. Input: Load image to segment
3. Normalize image to [0,1]
4. Create graph cut object for optimization
   4.1. Parameters: numLabels and numSites
   4.2. Create a handle fore this object
5. Set data cost: the cost of assigning label h to site i
6. Set smoothing cost: using Potts model
7. Set neighborhood structure with pairwise connectivity weights
   7.1. Weights(i,j)>0 := i and j are neighbors
8. Perform $\alpha - expansion$
9. Reshape into image: use matlab 'reshape(labeling, x,y,z)'
10. Output: Energy = data energy + smooth energy and matrix of segmented label assignments

---

3.3 Related Work

Graph cut optimization methods have been used in a variety of problems within the imaging community. The rigor of this process has been well recognized as an efficient technique for energy minimization, applied to image restoration [62] [67], synthesis [68], and segmentation [61] [69] to name a few. A variety of fields, such as tumor extraction [70], focal cortical dysplasia (a malfunction of neurons often linked with seizures)[71], and skull stripping[72] used graph cuts in recent studies.

Chapter 4

Motivations, Materials, and Methods Used

This chapter states our research goals, and motivations, with developing this study. The materials section states the software and additional libraries used throughout the process of collecting, calculating, and analyzing data. The methods section goes in depth with some of the procedures required to complete our work.

4.1 Motivation

This study was driven by a fascination for the brain as well as graph theory. Our objective was to compare grey matter volume estimation from MRI images as done within SPM versus as computed using

graph cut segmentation to identify the grey matter regions. Thus, how do graph-cuts based volume calculations differ from SPM based results? Throughout our study we focused much of our attention on answering, what parameters most impact these graph cuts based results?

We recognize SPM is a popular pipeline and graph cuts are a newer accepted tool in the neuroimaging field. When considering the robustness of alternate approaches, the accuracy and efficiency of graph cuts proved to be not only reliable but flexible with its current and potential applications[63]. This allowed us to consider using the multi-label optimization techniques similar to those given by [66] for our study.

The main advantages of our research over the numerous papers published in the literature are as follows (1) we have provided further insight on the inclusion of graph theoretic approaches when studying the brain through relevant data analysis (2) we have proposed a unique longitudinal analysis for clinical application demonstrating proactive research rather than responsive research.

Our work involved head and brain segmentation, processing, and interpretation. The underlying clinical motivation was investigating GM volume changes in the MRI scans across a spectrum of previously declared “healthy” subjects (several of whom will have abnormalities found in their future MRI scans). For instance picture a radiologist defining a brain as healthy then two years later defining a scan of the same patient as abnormal. At what point is the abnormality detectable? Perhaps there were signs at the earlier scan that were not sought out. This is where our research comes into play. We compare grey matter volume estimation as done within SPM versus as computed using graph cut segmentation to identify the grey matter regions. We propose after examining potential GM differences, choosing yet another region of the brain to seek potential differences.

Each brain region with or without detectable volume changes lends itself to future research advancements in the field.

4.2 BrainWeb

Twenty T1 normal anatomical normal brain simulations were used separately (181x256x256 voxels of size 1x1x1mm^3).

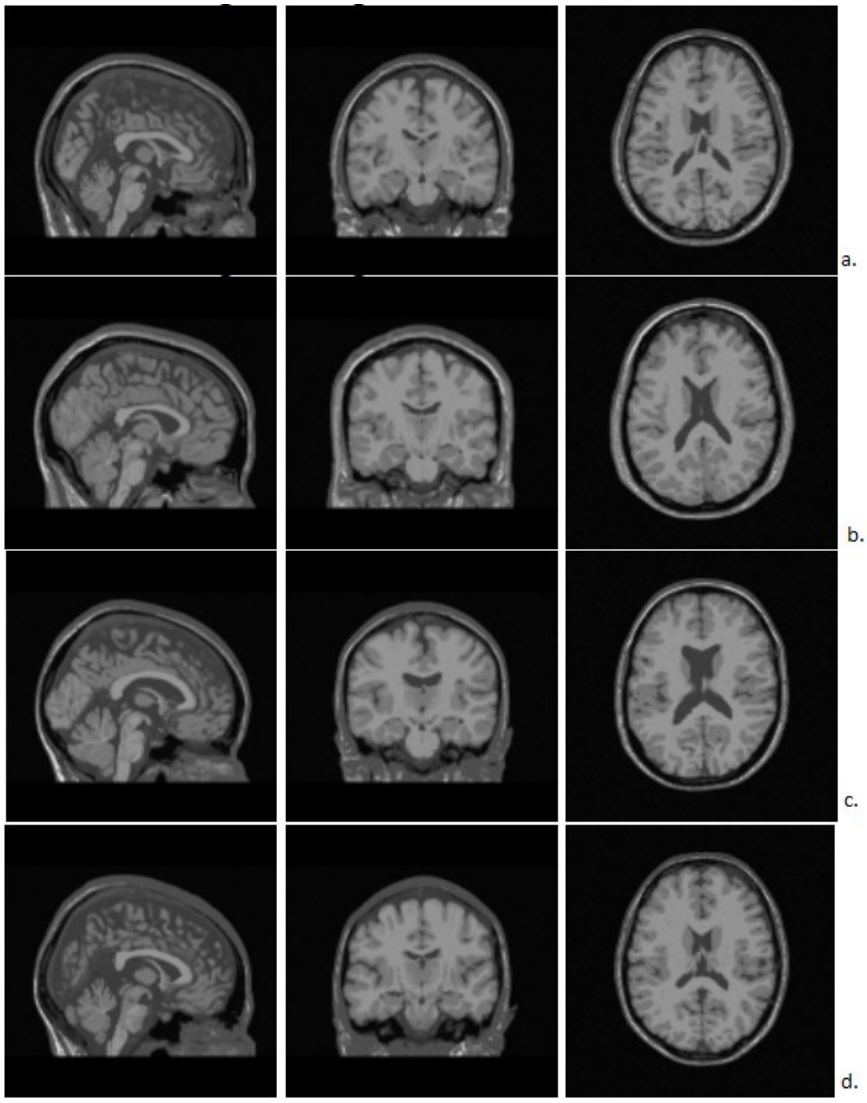

Figure 21.[1] examples of T1 anatomical brain simulations, from top down (a-d) respectively: case number 1- subject 04; case number 3- subject 06; case number 11- subject 45; case number 17- subject 51;

These MRI datasets were used from the internet connected BrainWeb system (http://brainweb.bic.mni.mcgill.ca/brainweb/). These simulated datasets, as shown in Figure 21, are produced by the MRI simulator at the McConnell Brain Imaging Centre in Montreal and are frequently used by the neuroimaging community to evaluate performance and validity of techniques in research. The datasets are based on an anatomical model of a normal brain in combination with a set of 3-dimensional "fuzzy" tissue membership volumes, one for each tissue class (WM, GM, CSF, fat, skin, etc). Voxel values reflect the proportion [0, 1] of each tissue type represented and an MR simulation provides a realistic contrast of the image and intensities. This real-like MR simulation is represented through signals predicted by a Bloch equation based discrete-event simulation pulse sequences[1], [73], [74], [75]. Bloch equations are a set of macroscopic equations which replicate the nuclear magnetization motion of, in this case, MRI machine computed scans.

BrainWeb simulated models have been used in many scientific and mathematical contexts surrounding studies involving MRI data - method evaluation, qualitative and quantitative volume analysis, reconstruction of brain structures, and more [76][77][78][42].

4.3 SPM

Statistical Parametric Mapping 8 (SPM8) [21] was used with MATLAB 7.11.0 (R2010b)[79]. Utilities including spatial normalization, grey matter tissue segmentation, modulation, and smoothing were amongst those used as part of the VBM preprocessing described in Chapter 2 for calculating volume as described in section 4.7.

4.4 BrainSuite

As the process stands, the image analysis stage of skull stripping or "brain extraction" was completed with BrainSuite13[80] software. All original T1 normal brain brainWeb simulated MRI images were processed using default values deliberately to evaluate the accuracy of results from a non-expert user. BrainSuite has an automatic sequence for cortical extraction of T1 MRI images, which utilizes a Brain Surface Extractor (BSE) operating by Marr-Hildreth edge detection.

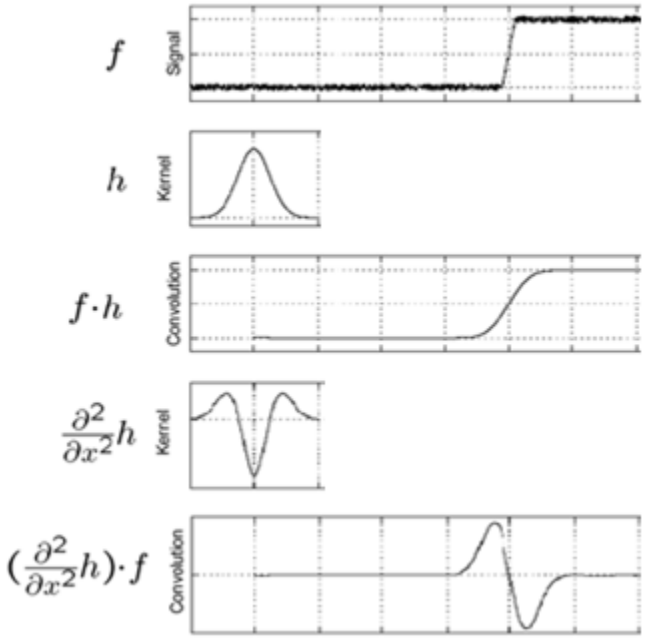

Figure 22. For example, from top down demonstrated the results of the Marr-Hildreth process: The noisy original signal represents the original image function; *h* represents the Gaussian kernel used to smooth the signal; the remaining convolution is the Gaussian smoothed signal; next we have the second derivative Laplacian of the Gaussian or Laplacian of the Gaussian (LoG); Lastly, on the bottom, we have the LoG of the signal where the zeros (at x=1000) predict the existing edge(s) of the original function.

Marr-Hildreth edge detection here is based on the following main ideas and is demonstrated in Figure 22.

1. A T1 image has strong edges due to the high contrast between the CSF and the brain tissue or skull.
2. A Gaussian operator smoothes the image, to reduce errors due to noise.
3. The zero-crossings of the Laplacian of the image represent step differences in the intensity of the original image, thus, the edges to be detected can be estimated with linear interpolation.

BrainSuite13a software is available at UCLA Laboratory of Neuro Imaging[80]. Skull stripping, skull and scalp, and nonuniformity correction were the extraction stages utilized in this study.

4.5 Brain Masking

Throughout the process of calculating GM volumes using the BrainSuite skull stripping procedure, we found more applicable results by creating our own brain masks and stripping the skull from our computations. This process created a mask for each subject by, first, taking the union of SPM generated GM and WM segmented normalized images. Second, we binarized the masks and performed morphological operations specifically dialation followed by erosion (or ‘closing’) to rid any holes (undefined regions in the brain) and obtain a mask. Third, calculating the intersection of this mask and a normalized T1 full brain scan provides the skull-stripped image. Similar to the MNI process (described in Figure 4) of utilizing atlases to create masks, our masks are subject specified and defined. Brain masking was practical for our study, as we had a sample size that could support it and a goal best fit by requiring its results.

We found this process, when used, eliminated other factors (such as different normalization methods, different skull stripping methods, etc.) beyond the graph-cuts and SPM segmentation stages we looked to compare, in GM volume calculation process.

4.6 Graph Cuts Library

Starting with a skull stripped image we were able to normalize, segment, and smooth the images using a graph cuts library for optimizing multi-label energies (see chapter 5 for more detail of the procedure and results). The $\alpha - expansion$ algorithm was applied as defined in section 3.2.2 and called in the graph cuts segmentation script that proceeded as described in section 3.2.2.

4.7 Volume

4.7.1 Ground Truth

The "ground truth" gray matter volume for each subject was calculated using the individual BrainWeb grey matter "fuzzy" models.

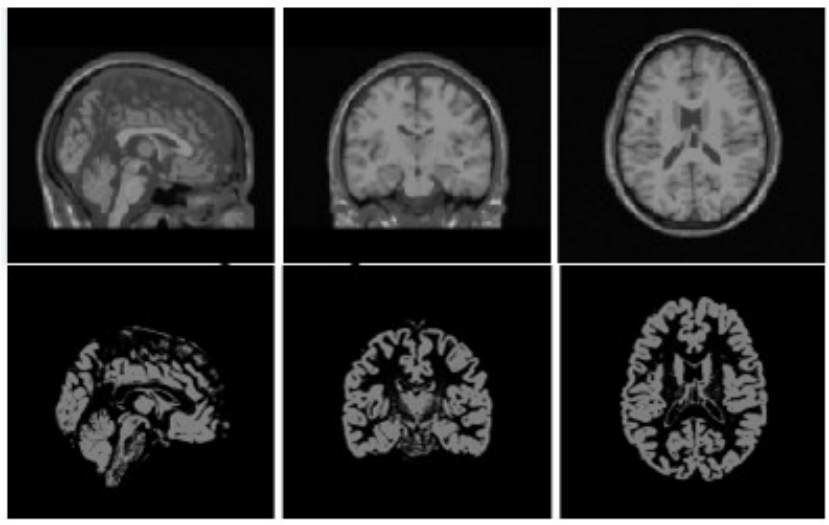

```
image dimensions: zspace yspace xspace
    dimension name         length         step         start
    --------------         ------         ----         -----
    zspace                    181            1       -72.25
    yspace                    256            1      -145.75
    xspace                    256            1      -127.75
```

Figure 23. [2] BrainWeb Subject 04 T1 simulated full image and grey matter image

4.7.2 Volume Calculation

BrainWeb images have defined dimensions and step length measurements. For instance, the simulated MRI image in Figure 23 is defined as 256x256x181 and one voxel as 1x1x1 mm^3. Thus, the volume, V_T, [45][55] can be calculated in litres by, the number of voxels, *n,* and the voxel volume, *v.*

$$V_T = v \cdot n$$

$$V_T = (s_x \cdot s_y \cdot s_z)/100^3) \cdot E_L$$

$$n = \sum_{i=1}^{181} E_L^i = E_L$$

$$v = (s_x \cdot s_y \cdot s_z)/C$$

$$v = (s_x \cdot s_y \cdot s_z)/100^3, \quad C = 100^3$$

where,

$s_x = 1,\ s_y = 1,\ s_z = 1$

For the step size given in each dimensional direction, and, C is the constant of conversion from mm^3 to litres . E_L^i provides the number of elements in the image slice i with labeling L leaving $E_L$to serve as the summation, or total, number of elements in the 3D image with label L. Computationally, the following shows the algorithm used for calculating the volume. Notice, when dealing with a 3D matrix, M, with desired label L, step one can be replaced with the 'find(M==L)' function in MATLAB rather than looping through each slice.

Algorithm: Volume

1. For each slice $s \leq$ number of slices
   1.1. Get the number of voxels of the slice
   1.2. Sum $\coloneqq$ Sum + (number of voxels of the slice)
2. Calculate the voxel-volume using given step sizes and convert mm^3 to litres
3. Solve total volume $\coloneqq$ Sum * voxel-volume

4.7.3 GM Volume: SPM

The volume algorithm above incorporated preexisting SPM functions and formatting to maintain full effectiveness. The volume was calculated on the SPM pipeline saved output images that were smoothed, modulated (as well as not modulated), segmented, and normalized (process described in Chapter 2). All images were processed using default values intentionally to evaluate the accuracy of a non-expert user.

4.7.4 GM Volume: Graph Cuts

All GM volumes calculated from whole brains, using the graph cut technique described in section 4.6. Skull stripped images were performed using BrainSuite described in section 4.4, as well as using the brain masking process described in section 4.5. The volume algorithm described above was performed on the skull stripped, normalized, segmented, smoothed resulting images.

Chapter 5

Results

In this study, we chose to examine the GM volume calculations of 20 normal anatomical normal brain BrainWeb images using MATLAB with a graph-cuts based approach and an SPM approach. In doing so, we aimed to conduct a comparative analysis specifically on the segmentation stage of these methodologies. We obtained the results shared in this chapter.

5.1 BrainWeb – Ground Truth

As described earlier, ground truth (GT) values were calculated from the BrainWeb given grey matter segmentation images. These values were used in the following results. These results (see Table 2)

demonstrate, for this subject pool, an average brain volume of 0.9685 litres.

Case no.	Subject Number	Volume (*l*)
1	subject04_gm_v	**0.932824**
2	subject05_gm_v	**0.978909**
3	subject06_gm_v	**0.896322**
4	subject18_gm_v	**1.04442**
5	subject20_gm_v	**0.980805**
6	subject38_gm_v	**0.995723**
7	subject41_gm_v	**1.009684**
8	subject42_gm_v	**1.017752**
9	subject43_gm_v	**1.092941**
10	subject44_gm_v	**0.989154**
11	subject45_gm_v	**0.925454**
12	subject46_gm_v	**0.960003**
13	subject47_gm_v	**0.971913**
14	subject48_gm_v	**0.875739**
15	subject49_gm_v	**0.904392**
16	subject50_gm_v	**0.897895**
17	subject51_gm_v	**0.937677**
18	subject52_gm_v	**0.963992**
19	subject53_gm_v	**1.026874**
20	subject54_gm_v	**0.968243**

Table 2. Table of ground truth (GT) dataset from BrainWeb grey matter

5.2 SPM

SPM preprocessing stages were performed both with and without modulation. Recall, modulation scales the segmented normalized image by the amount of contraction or expansion to compensate for the effects of spatial normalization, allowing quantifiable results to be

the same as in the original image. Volumes calculated can be found in Table 3.

Case no.	**Subject Number**	**Volume (*l*) Incl. Mod.**	**Volume (*l*)**	**GT Vol. (*l*)**
1	subject04_t1w	0.870530	0.87366	**0.932824**
2	subject05_t1w	0.898929	0.90240	**0.978909**
3	subject06_t1w	0.876049	0.87937	**0.896322**
4	subject18_t1w	0.911092	0.91427	**1.04442**
5	subject20_t1w	0.901361	0.90478	**0.980805**
6	subject38_t1w	0.883913	0.88764	**0.995723**
7	subject41_t1w	0.877452	0.88057	**1.009684**
8	subject42_t1w	0.930534	0.93389	**1.017752**
9	subject43_t1w	0.888986	0.89207	**1.092941**
10	subject44_t1w	0.901906	0.90525	**0.989154**
11	subject45_t1w	0.899755	0.90352	**0.925454**
12	subject46_t1w	0.916772	0.91993	**0.960003**
13	subject47_t1w	0.826873	0.83042	**0.971913**
14	subject48_t1w	0.877106	0.88081	**0.875739**
15	subject49_t1w	0.804180	0.80737	**0.904392**
16	subject50_t1w	0.816204	0.81892	**0.897895**
17	subject51_t1w	0.887799	0.89089	**0.937677**
18	subject52_t1w	0.884869	0.88849	**0.963992**
19	subject53_t1w	0.897731	0.901541	**1.026874**
20	subject54_t1w	0.903839	0.906494	**0.906494**

Table 3. This table is shows the ground truth data in comparison with the recorded values of the normalized, segmented, modulated, and smoothed images using the SPM pipeline (titled incl.mod.), and values of the normalized, segmented, and smoothed images using the SPM pipeline.

An interesting observation included the comparison between images with the 'normal' preprocessing stages (normalization, segmentation, and smoothing) and those with modulation before smoothing (see Table 3). Both calculations under-estimate the GM volume, results of the processed images including modulation demonstrated an average of 0.0033 liters lower than the results calculated on the images processed with no modulation. With the intent to run SPM processes by default settings, these under estimates may be due an over compensation of scaling while modulating, an under expansion during normalization, or a lack of classification during segmentation.

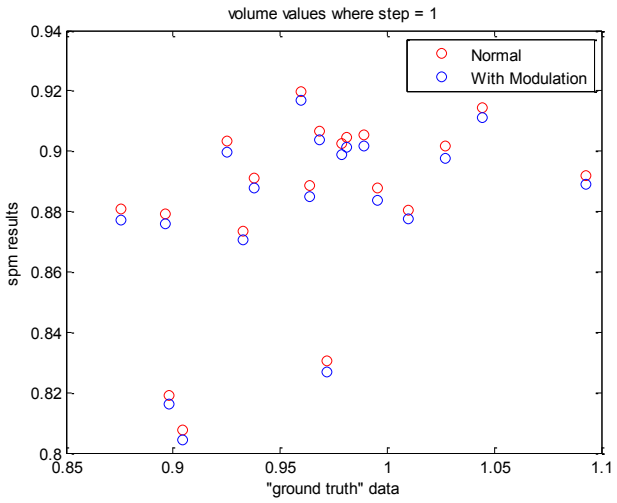

Figure 24. The volume of the GM segmented images with modulation demonstrated lower approximations compared with the images processed with no modulation stage.

5.3 Graph Cuts

All segmentation label values were collected based on the independent images. The graph cuts process of normalizing, segmenting, and smoothing images exemplified over-approximations of volume quantities. With a smoothing weight, s, of 0.0001 and data weight, dw, 1000-100000 these estimations had an average over approximation of 0.2655 litres. With a smoothing weight 0.001-

0.00001 and data weight 10000 these estimations had an average over approximation of 0.2694 litres. Recall the smoothing term is a constant used to set the pairwise connectivity weights between neighboring sites. This term scales the data weight value providing a constant lens to see the image boundaries/labels by.

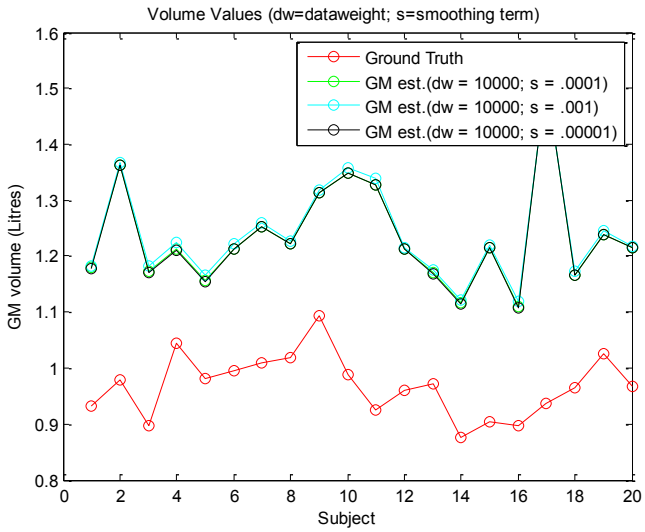

Figure 25. The GT volume values exists below the GM volume values from graph cuts segmentation process. The lower the smoothing term, s, the closer the volume estimate is to the GT value.

Qualitatively, the smaller the smoothing term, s, the more detailed the segmentation looks we see, with a certain data weight, the lower the smoothing weight value and the more definition in the solution of labeled GM. Consequently, the closer the GM volume estimate is to the GT. For values of dw ranging 1000-100,000 and s ranging from .00001-.001 we saw small variation in the GM volume estimates. Thus, we decided to alter additional parameters. We hypothesize (using qualitative and quantitative results several of which are exemplified in Figure 26,Figure 27, and Table 4) the over estimation from our graph cuts process as one that has misclassified GM as well as contains skull residue(small amounts of non-brain tissue remaining in the GM segment). Observing misclassifications between GM and other brain matter (see Figure 26) we decided to handle the label

values and strip the skull using subject based masks (as described in section 4.5).

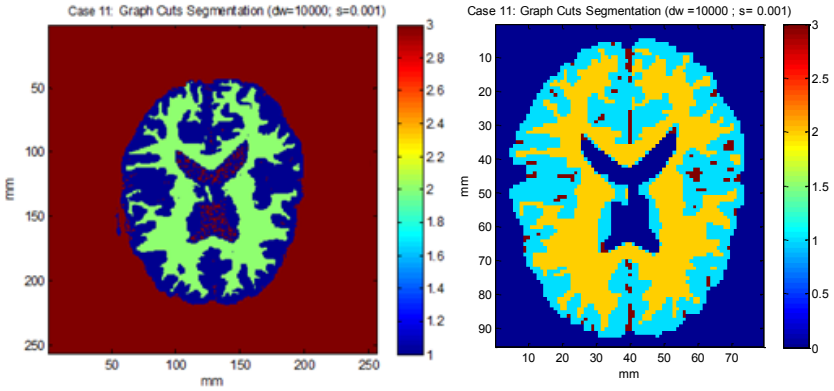

Figure 26. The two figures provide a visual for misclassified data. We can see in the left figure there is significantly more brain matter classified as GM (GM has scale value of 1)

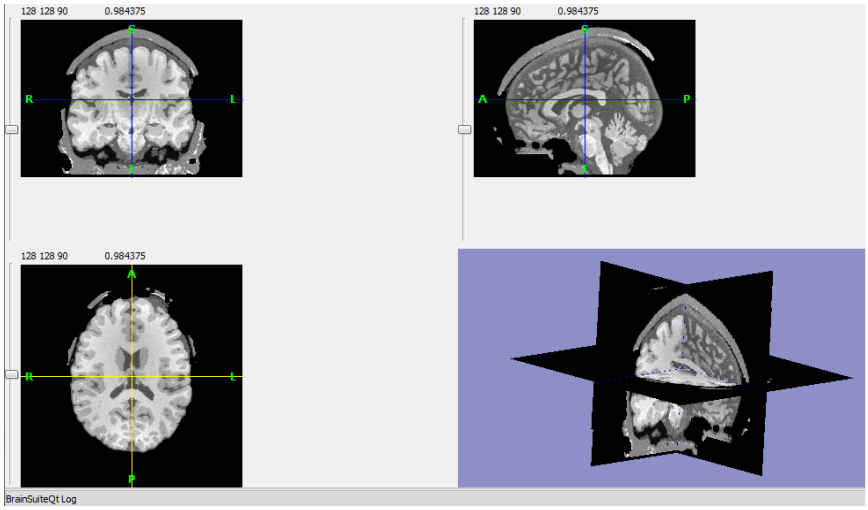

Figure 27. BrainSuite[80] interface coronial (upper left), axial (lower left), and sagittal (upper right) views demonstrating intense skull residue from subject case no. 17 (noted as an extreme outlier).

The following confusion matrix (Table 4) represents the GM classification from the graph cuts based process. It demonstrates 2139249.93 of the 11862016 voxels, or a ratio of almost 1/5 (specifically 0.180345 voxels), as being incorrectly classified GM.

$$\begin{bmatrix} 7748286.23 & 0 \\ 2139249.93 & 1974479.84 \end{bmatrix}$$

Table 4. The above confusion matrix demonstrates the true positives (upper left), false negatives (upper right), false positives (lower left), and true negatives (lower right) of the voxel count assignments from the graph cuts methods

Originally the three segmentation label values were declared based upon individual subject image intensities for WM, GM and a value of zero for "background" or "other." We noticed the volume values calculated using these labels were over approximations. Classifications for background were easily misclassified as GM, as the threshold deviated from the desired GM intensity range (see Figure 28, the over approximation is due to the misclassified intensities between the desired threshold boundary u and the current one u*).

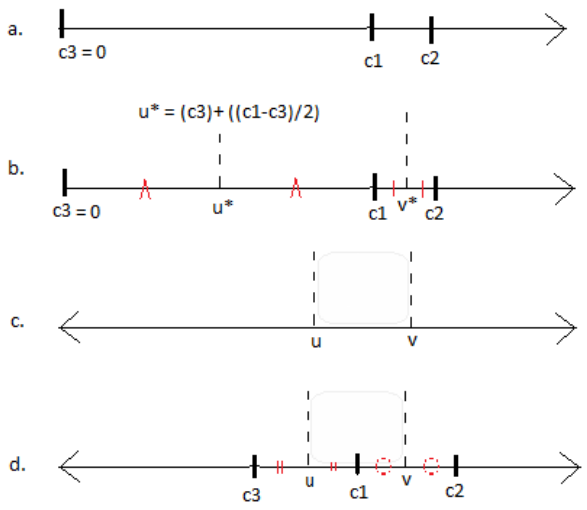

Figure 28. The above figure shows the segmentation thresholds as dependent upon the label values. (a) Exemplifies the original labels where c1 and c2 represent the GM and WM image pixel intensities (c1,c2 >0), respectively, and c3=0 for "background." (b) Displays the resulting thresholds with dashed lines. All intensities found to be lower than u* will

be classified with label c3, intensities found between u* and v* will be labeled as GM and those found to be greater than v* are WM. (c) Demonstrates the desired threshold for GM classification labels (values between u and v). (d) Produces the label values to obtain the GM classification threshold from (c).

Calculating the desired threshold boundaries, u and v, allowed us to utilize symmetry (about u and v), distance (between u and v as well as labels), and preciseness (of labels as observed when predetermining the intensity values). The following figure (Figure 29) demonstrates the GM volume calculated from the GT, SPM, as well as several different label classifications with graph cuts.

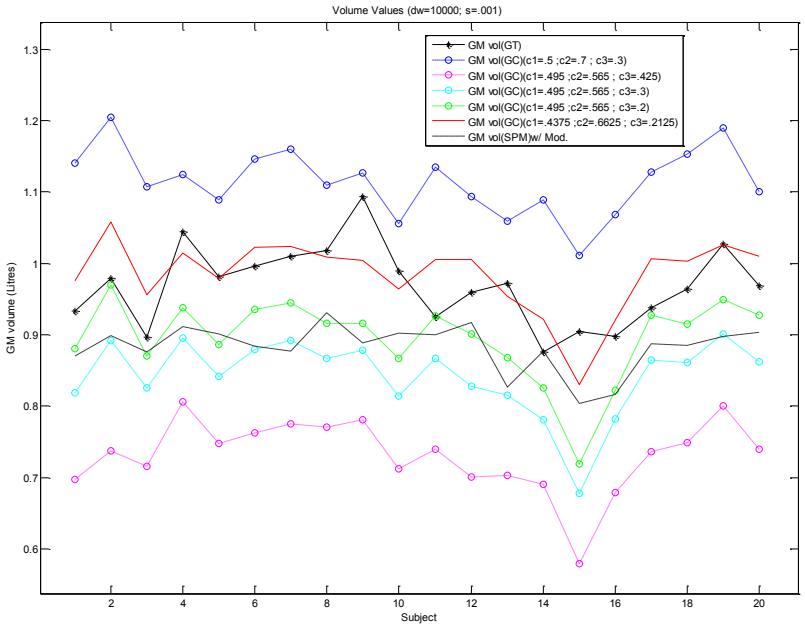

Figure 29. The GM volume calculated from the GT, SPM, as well as several different label classifications with graph cuts, as specified in the legend.

The amended study provided results that proved our hypothesis of misclassification and included skull residue, true. See appendix III for further information regarding parameter adjustments.

5.4 Confusion Matrix

The following confusion matrix (Table 5) represents the GM classification from the graph cuts based process. It demonstrates 128155 of the 11862016 voxels, or a ratio of near 1/100 as being incorrectly classified GM. Table 6, suggests almost 55 times that amount of misclassified voxels, is incorrectly labeled as 'other matter'.

$$\begin{bmatrix} \mathbf{7748286} & \mathbf{0} \\ \mathbf{128155} & \mathbf{3985574} \end{bmatrix}$$

Table 5. The above confusion matrix demonstrates the true positives (upper left), false negatives (upper right), false positives (lower left), and true negatives (lower right) of the voxel count assignments from the final graph cuts process (including brain masking and label corrections).

$$\begin{bmatrix} \mathbf{709747.77} & \mathbf{7038538.46} \\ \mathbf{0} & \mathbf{4113729.77} \end{bmatrix}$$

Table 6. The above confusion matrix demonstrates the true positives (upper left), false negatives (upper right), false positives (lower left), and true negatives (lower right) of the voxel count assignments from the SPM preprocessing.

The methods we evaluated, graph cuts and SPM based, classify GM voxels with 99% and 89% accuracy, respectively. Where, TP = true positive, FP = false positive, FN = false negative, and TN = true negative, accuracy, a, is defined:

$$a = ((TP/(TP + FP)) + (TN/(TN + FN)))/2$$

The sensitivity values, *SN*, or the ability to identify positive results were calculated and reported:

$$SN = TP/(TP + FN)$$

$$SN_{Graph\ Cuts} = 1$$

$$SN_{SPM} = 0.0916$$

And the specificity values, *SP*, or the ability to identify negative results were calculated and reported below:

$$SP = TN/(TN + FP)$$

$$SP_{Graph\ Cuts} = 0.4800$$

$$SP_{SPM} = 1$$

5.5 Comparisons

Both SPM and graph cuts estimation curves follow the GT value curve (see Figure 30). Subject case 17 was an outlier with graph cuts estimation before further skull stripping including 0.5 litres over the GT. While SPM under estimates by 0.0844 litres, our graph cuts technique maintains an average difference in estimated GM volume of 0.0407 litres. This halves the average difference found using SPM .

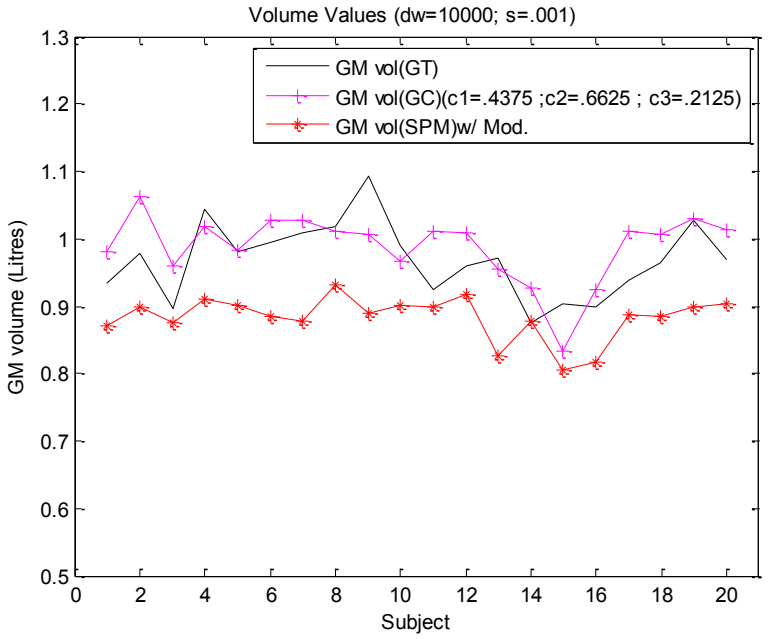

Figure 30. Volume values calculated after graph cuts (GC) process and SPM process relating to the ground truth (GT) volume values (the solid line). Refer to the legend for more information. See Appendix III for more information regarding parameter adjustments)

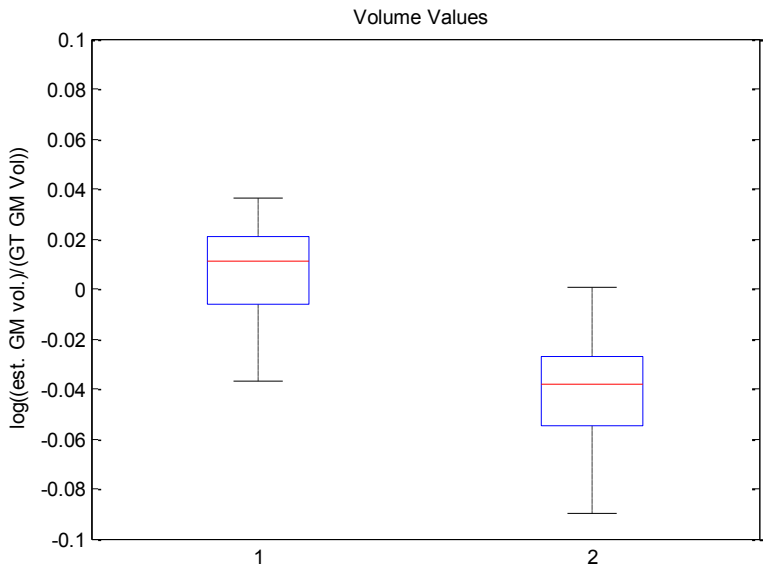

Figure 31. The above figures demonstrate (1) the graph cuts volume estimates and (2) the SPM volume estimates. Notice, y = log((estimated GM volume)/(GT GM volume)), thus, graph cuts is significantly closer to zero than SPM (signifying accuracy in GM volume estimates)

When analyzing these results, the graph cuts technique out performs the SPM process. Visually, the differences in the estimated GM using SPM, GM using graph cuts, and ground truth GM are minimal. Some visual cues displaying a lack of detail in the cortical regions including surface volumes of the cerebral hemispheres is noticeable.

Both processes (graph cuts and SPM based) successfully include parts of the cerebellum, cerebral hemispheres specifically cerebral cortex (with segmentation parameter dependency), the cerebrum (thalamus, hypothalamus: subthalamus, basal ganglia, etc.), and cerebellar nuclei. However (see Figure 31), calculations show mean errors of 0.0407 litres for graph cuts based approximation and -0.08408 litres for SPM based approximation.

Chapter 6

Discussion

6.1 Conclusions

MRI scans are particularly sensitive to data collection (machines, peripherals, and processing)[3], [4]. This study confirmed the importance of utilizing the same process when calculating data; by supplying results that are comparable only within the same preprocessing procedure. We recognize SPM is a more common procedure for processing but see the positive potential in further research and application of graph theoretic approaches.

Both estimations are imprecise, with relative error percentages of 1.6% and 8.4% for graph cuts and SPM procedures respectively. Many studies recognize the interior GM voxels to have similar

intensities to those of white matter and brain surface voxels have near indistinguishable intensities from the skull[42].

From the evaluation and analysis performed throughout this study, we do not share any further information on the correlation between a specific process and a specific application.

6.2 Future Work

First, we endorse further investigation and application of graph cuts (and other graph theoretic tactics) in neuroimaging. This is a well needed and, currently, supported[81] new approach to studying the brain- its mapping and its processing.

One of the main challenges with the MRI image process is the consistency with input and output data formats. A challenge we faced in this study that we recommend further investigation includes the format of the current graph cuts segmentation process (see Chapter 3). A form friendly to SPM–preprocessing will allow for additional investigation of specific stages of the graph cuts preprocessing course. Rather than the normalizing, segmenting, and smoothing stages being lumped and compared to SPM preprocess as a whole. The thought is, by narrowing the focus, we will be able to detect significant effects caused by specific stages. We accomplished this with a subject specific approach of which we encourage further advancement on.

As mentioned earlier, our intent was to complete the study using defaults settings for SPM. We recommend altering the base parameters of SPM as well as graph cuts parameters for further specificity is results.

Overall, GM volume changes are symptomatic and often indicative of a plethora of diseases and developmental processes. As we stated, one of the primary motives behind this study was the proposal and design of its clinical application.

A number of studies have explored brain atrophy, scrutinized approaches, and defined interesting future work. The Mind Research Network in Albuquerque, New Mexico has established an extensive network of scans (including MRI datasets). Obtaining clinical datasets will allow for an investigation of GM volume changes as follows. The proposed study will compare the healthy scans of 'x' subjects (controls) and comparing them with the "healthy" scans of 'y' subjects with whom have a later declaration of an abnormality (disease subjects) .We will examine for changes in the brain, specifically looking at the volume of grey matter to see if there is any significant difference between the healthy brains of the controls and the "healthy" brains of the disease subjects. If we think about a radiologist declaring a scan as normal, where normal means having no abnormalities, at what point will the radiologist be able to define an abnormality, after having insight on the future? After examining potential GM differences we recommend choosing yet another region of the brain to seek potential differences, as each region with or without detectable changes supply information to future research and advancements in the field. Thus, the inspiration behind this work is to create a longitudinal study being proactive rather than reactive (clinically speaking, preventative rather than responsive) see section 1.3 and selectively apply an efficient procedure for determining these results (utilizing graph cuts techniques or otherwise).

Acknowledgments

Many people have contributed to my successes and development throughout my graduate studies. First, I would like to express my gratitude to my advisor Dr. Nathan Cahill of the Applied and Computational Mathematics program at Rochester Institute of Technology (RIT). Dr. Cahill, is also a member of the Imaging Sciences program at RIT. His broad range of interests and professional skillset had me enthused to work with him. His natural ability to network was both informative and enjoyable. I am fortunate that he not only served as a resource for me, but gave me a valuable lesson of "taking a chill pill". My high-speed, high-energy, focus, and intensity did well by his more relaxed demeanor. I can only suggest that we not schedule our meetings at 9:00 in the morning!

Members of my thesis committee have been helpful through their guidance and support. Thank you to Dr. Darren Narayan who truly sparked my curiosity with our fascinating discussions of graph theoretic approaches to brain networking. And to Dr. Linwei Wang who provided valuable lessons, insight and knowledge in medical imaging. I am grateful to the RIT faculty for guiding my coursework and time here as a student. Particular members of the department who played special and unique roles include Dr. Coppenbarger, Dr. Shahmohamad, and Dr. Wiandt. These individuals added to my foundational knowledge, confidence, and creativity as a scholar.

A large expression of gratitude is extended to my family. My mother's strength, prayers, encouragement and kind words (as well as care packages) were always what I needed to get though a rough patch. When I would excel through a week, her ear was there to have me share all of my research ventures and reminding me that my father was looking down at me, proud. I am blessed for the inquisitiveness and strong work ethic instilled in me at a young age.

It seemed others' presence in my secluded lab regenerated the fuel needed to encourage my work. Osborn de Lima was another rock when I needed strength, he was upbeat when I felt my rhythm was off, and notably he was a great brainstorming partner. Many occasions of explaining my thoughts and mapping out ideas paid off (thank you to Mohammad Yousefhousien for being a great resource to discuss volume calculations).

Lastly,a big thank you goes out to my best friend Selin Sariaydin, my classmates, colleagues, and teammates without whom I would not have been as engaged in the community and consequently in my own learning. Academic and non-academic interactions helped me through my graduate life and success here at RIT.

Acronyms

(AD)	Alzheimer's disease
(byFTLD)	behavioral variant FTLD
(BSE)	Brain Surface Extractor
(BSI-UCD)	"Boundary Shift Integral" developed by Imaging of Dementia and Aging Lab., University of California, Davis
(CBB)	Cerebellum and brainstem
(CSF)	Cerebrospinal fluid
(DARTEL)	Diffeomorphic Anatomic Registration Through Exponentiated Lie
(EMS)	Expectations Maximization Segmentation
(FL)	Frontal lobe
(FN)	False negative
(FP)	False positive
(FTLD)	Frontotemporal lobar degeneration
(FWHM)	Full width half-maximum
(GLM)	General linear model
(GM)	Gray matter
(GT)	Ground truth
(HBSA)	Histogram-based segmentation algorithm
(IPCA)	iterative principal component analysis
(LCH)	left cerebral hemisphere
(LoG)	Laplacian of the Gaussian
(MNI)	Montreal Neurological Institute
(MRI)	Magnetic resonance imaging
(MTC)	Multispectral tissue classification
(NMR)	Nuclear Magnetic Resonance
(PF)	Prefrontal cortex
(POA)	Proportion of agreement
(PNFA)	Progressive nonfluent aphasia
(PVC)	Partial volume correction

(RAVENS)	Regional Analysis of Volumes Examined in Normalized Space
(RCH)	Right cerebral hemisphere
(SAD)	Social anxiety disorder
(semD)	Semantic dementia
(SIENAX)	SIENA extended to a cross-sectional method
(SPM8)	Statistical Parametric Mapping 8
(SRAN)	Self-adaptive Resource Allocation Network
(T1DM)	Type 1 diabetes mellitus
(TL)	Temporal lobe
(TN)	True negative
(TP)	True positive
(VBM)	Voxel-Based Morphometry
(WM)	White matter

Table of Figures

Included Tables

Appendix I – [46] Voxel Based Morphometry Preprocessing

Overview

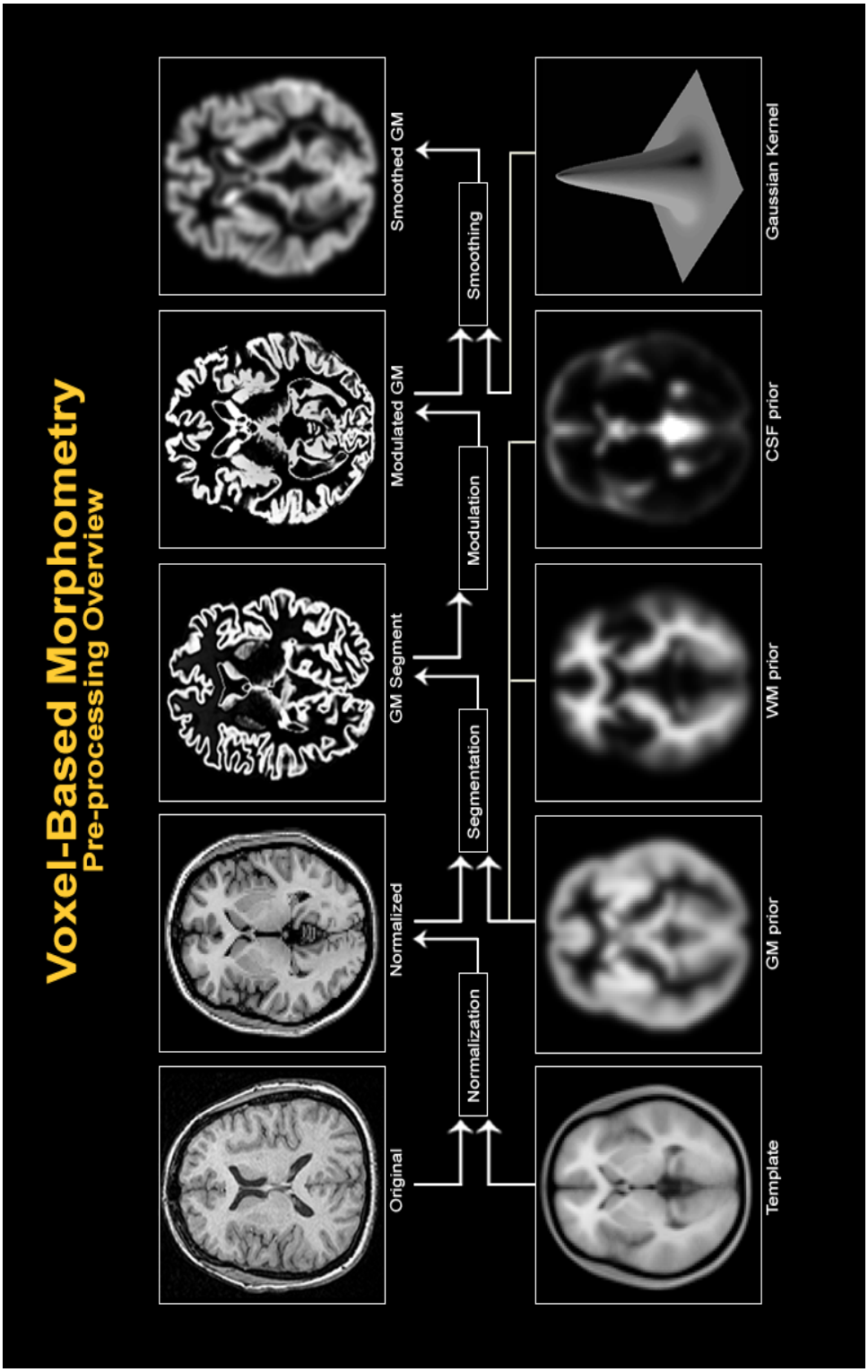

Appendix II – [52] Segmentation Techniques

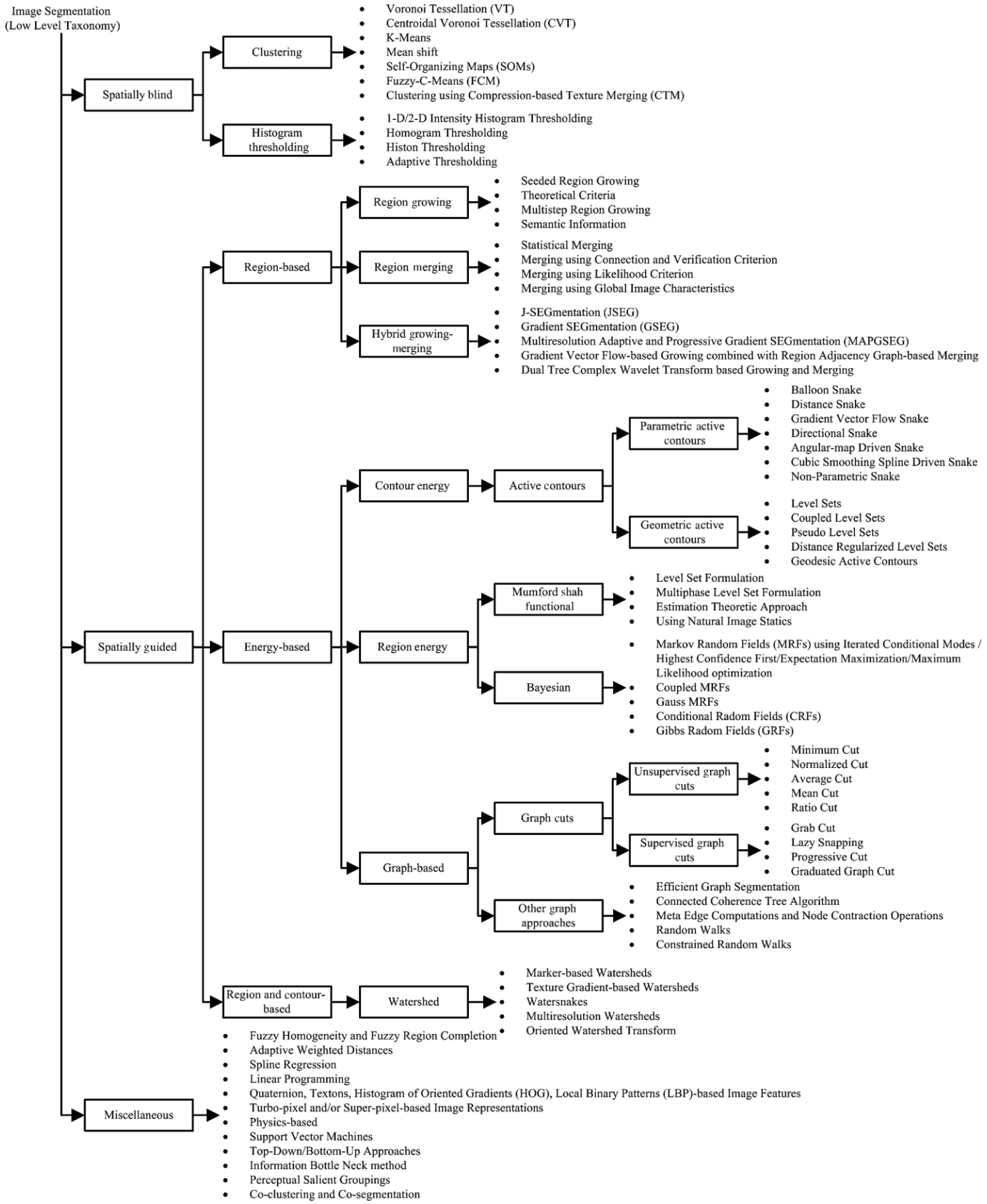

Appendix III -Volume Values (legend for parameter adjustments)

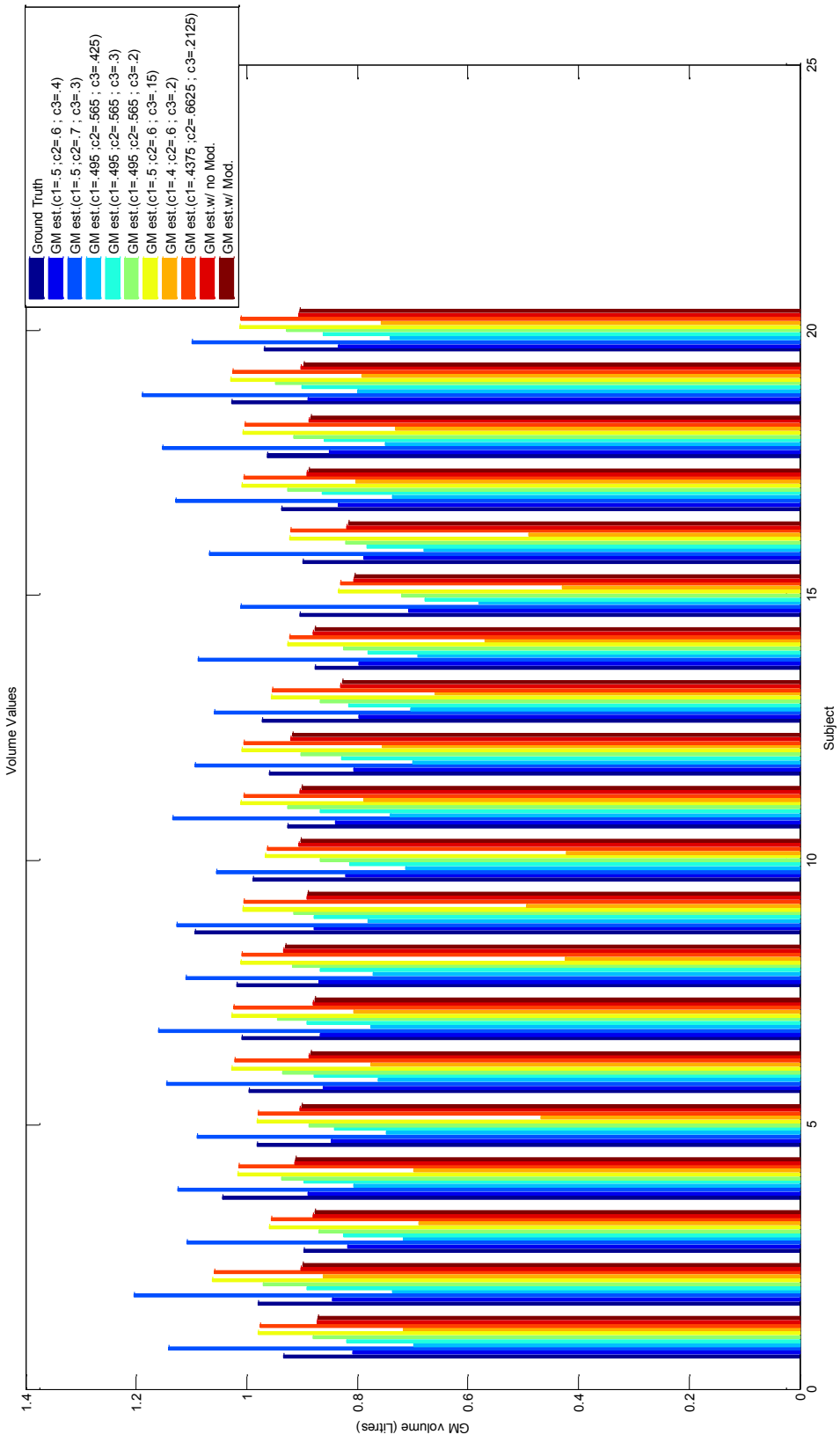

References

[1] C. A. Cocosco, V. Kollokian, R. K.-S. Kwan, and A. C. Evans, "Brainweb: Online interface to a 3D MRI simulated brain database.," *NeuroImage*, vol. 5, no. S425, 1997.

[2] "BrainWeb: Simulated Brain Database." [Online]. Available: http://brainweb.bic.mni.mcgill.ca/brainweb/. [Accessed: 17-Apr-2013].

[3] H. Zaidi, T. Ruest, F. Schoenahl, and M.-L. Montandon, "Comparative assessment of statistical brain MR image segmentation algorithms and their impact on partial volume correction in PET," *NeuroImage*, vol. 32, no. 4, pp. 1591–1607, Oct. 2006.

[4] M. Battaglini, S. . Smith, S. Brogi, and N. De Stefano, "Enhanced brain extraction improves the accuracy of brain atrophy estimation," *NeuroImage*, vol. 40, pp. 583–589, 2008.

[5] M. Schaer, R. Poryazova, S. Schwartz, C. L. Bassetti, and C. R. Baumann, "Cortical morphometry in narcolepsy with cataplexy," *J. Sleep Res.*, vol. 21, no. 5, pp. 487–494, Oct. 2012.

[6] Freesurfer package, Martinos Center for Biomedical Imaging, Massachusetts General Hospital, Boston, MA, USA., http://surfer.nmr.mgh.harvard.edu/.

[7] J. E. Peelle, R. Cusack, and R. N. A. Henson, "Adjusting for global effects in voxel-based morphometry: Gray matter decline in normal aging," *NeuroImage*, vol. 60, no. 2, pp. 1503–1516, Apr. 2012.

[8] D. J. Cobia, M. J. Smith, L. Wang, and J. G. Csernansky, "Longitudinal progression of frontal and temporal lobe changes in schizophrenia," *Schizophr. Res.*, vol. 139, no. 1–3, pp. 1–6, Aug. 2012.

[9] J. S. Kim, C. K. Chung, H. J. Jo, J. M. Lee, and J. S. Kown, "Regional thinning of cerebral cortical thickness in first-episode and chronic schizophrenia," *Int. J. Imaging Syst. Technol.*, vol. 22, no. 1, pp. 73–80, Mar. 2012.

[10] A. B. Whitworth, M. Honeder, C. Kremser, G. Kemmler, S. Felber, A. Hausmann, C. Wanko, H. Wechdorn, F. Aichner, C. H. Stuppaeck, and W. . Fleischhacker, "Hippocampal volume reduction in male schizophrenic patients," *Schizophr Res*, no. 31, pp. 73–81, 1998.

[11] V. Molina, J. Sanz, F. Sarramea, C. Benito, and T. Palomo, "Lower prefrontal gray matter volume in schizophrenia in chronic but not in first episode schizophrenia patients," *Psychiatry Res*, no. 131, pp. 45–56, 2004.

[12] A. Mechelli, C. Price, K. Friston, and J. Ashburner, "Voxel-Based Morphometry of the Human Brain: Methods and Applications," *Curr. Med. Imaging Rev.*, vol. 1, no. 2, pp. 105–113, Jun. 2005.

[13] B. S. Mahanand, S. Suresh, N. Sundararajan, and M. Aswatha Kumar, "Identification of brain regions responsible for

Alzheimer's disease using a Self-adaptive Resource Allocation Network," *Neural Netw.*, vol. 32, pp. 313–322, Aug. 2012.
[14] S. Modi, M. Bhattacharya, N. Singh, R. P. Tripathi, and S. Khushu, "Effect of visual experience on structural organization of the human brain: A voxel based morphometric study using DARTEL," *Eur. J. Radiol.*, vol. 81, no. 10, pp. 2811–2819, Oct. 2012.
[15] D. C. Perantie, J. M. Koller, P. M. Weaver, H. M. Lugar, K. J. Black, N. H. White, and T. Hershey, "Prospectively Determined Impact of Type 1 Diabetes on Brain Volume During Development," *Diabetes*, vol. 60, no. 11, pp. 3006–3014, Sep. 2011.
[16] Z. Chen, L. Li, J. Sun, and L. Ma, "Mapping the brain in type II diabetes: Voxel-based morphometry using DARTEL," *Eur. J. Radiol.*, vol. 81, no. 8, pp. 1870–1876, Aug. 2012.
[17] G. Kalpouzos, G. Chételat, J.-C. Baron, B. Landeau, K. Mevel, C. Godeau, L. Barré, J.-M. Constans, F. Viader, F. Eustache, and B. Desgranges, "Voxel-based mapping of brain gray matter volume and glucose metabolism profiles in normal aging," *Neurobiol. Aging*, vol. 30, no. 1, pp. 112–124, Jan. 2009.
[18] M. Battaglini, M. Jenkinson, and N. De Stefano, "Evaluating and reducing the impact of white matter lesions on brain volume measurements," *Hum. Brain Mapp.*, vol. 33, no. 9, pp. 2062–2071, Sep. 2012.
[19] D.-P. Streitbürger, H. E. Möller, M. Tittgemeyer, M. Hund-Georgiadis, M. L. Schroeter, and K. Mueller, "Investigating Structural Brain Changes of Dehydration Using Voxel-Based Morphometry," *Plos One*, vol. 7, no. 8, p. e44195, Aug. 2012.
[20] L. Garrido, N. Furl, B. Draganski, N. Weiskopf, J. Stevens, G. C.-Y. Tan, J. Driver, R. J. Dolan, and B. Duchaine, "Voxel-based morphometry reveals reduced grey matter volume in the temporal cortex of developmental prosopagnosics," *Brain*, vol. 132, no. 12, pp. 3443–3455, Nov. 2009.
[21] *SPM- Statistical Parametric Mapping*. http://www.fil.ion.ucl.ac.uk/spm/.
[22] *MNI - Montreal Neurological Institute*. http://www.bic.mni.mcgill.ca/ServicesAtlases/ICBM152NLin2009.
[23] "DARTEL | Neurometrika." [Online]. Available: http://www.neurometrika.org/node/34. [Accessed: 23-Apr-2013].
[24] R. Oostenveld, P. Fries, E. Maris, and J.-M. Schoffelen, "FieldTrip: Open Source Software for Advanced Analysis of MEG, EEG, and Invasive Electrophysiological Data," *Comput. Intell. Neurosci.*, vol. 2011, pp. 1–9, 2011.
[25] S. Syal, C. J. Hattingh, J.-P. Fouché, B. Spottiswoode, P. D. Carey, C. Lochner, and D. J. Stein, "Grey matter abnormalities in social anxiety disorder: a pilot study," *Metab. Brain Dis.*, vol. 27, no. 3, pp. 299–309, Apr. 2012.

[26] A. M. Winkler, P. Kochunov, J. Blangero, L. Almasy, K. Zilles, P. T. Fox, R. Duggirala, and D. C. Glahn, "Cortical thickness or grey matter volume? The importance of selecting the phenotype for imaging genetics studies," *NeuroImage*, vol. 53, no. 3, pp. 1135–1146, Nov. 2010.

[27] "nucleus_caudatus.jpg (JPEG Image, 474 × 328 pixels) - Scaled (0%)," 2007. [Online]. Available: http://img.tfd.com/dorland/nucleus_caudatus.jpg. [Accessed: 23-Apr-2013].

[28] Y. Zhang, J. C. H. Chu, W. Hsi, A. J. Khan, P. S. Mehta, D. B. Bernard, and R. A. Abrams, "Evaluation of Four Volume-Based Image Registration Algorithms," *Med. Dosim.*, vol. 34, no. 4, pp. 317–322, Dec. 2009.

[29] D. Wang and D. M. Doddrell, "MR image-based measurement of rates of change in volumes of brain structures. Part I: method and validation," *Magn. Reson. Imaging*, vol. 20, no. 1, pp. 27–40, Jan. 2002.

[30] S. Sharma, V. Noblet, F. Rousseau, F. Heitz, L. Rumbach, and J.-P. Armspach, "Evaluation of brain atrophy estimation algorithms using simulated ground-truth data," *Med. Image Anal.*, vol. 14, no. 3, pp. 373–389, Jun. 2010.

[31] A. M. Michael, "IMAGING SCHIZOPHRENIA: DATA FUSION APPROACHES TO CHARACTERIZE AND CLASSIFY," Rochester Institute of Technology- College of Science, Chester F. Carlson Center for Imaging Science, 2009.

[32] T. Servoss, "Collection and analysis of multispectral magnetic resonance imaging data using a clinical imaging system," Rochester Institute of Technology- College of Science, Chester F. Carlson Center for Imaging Science, 2001.

[33] N. Narendranath, "Optimization of slice thickness in multispectral MRI tissue classification of brain tissues," Rochester Institute of Technology- College of Science, Chester F. Carlson Center for Imaging Science, 1996.

[34] J. Ashburner, "A fast diffeomorphic image registration algorithm," *NeuroImage*, vol. 38, no. 1, pp. 95–113, Oct. 2007.

[35] L. Frings, I. Mader, B. G. Landwehrmeyer, C. Weiller, M. Hüll, and H.-J. Huppertz, "Quantifying change in individual subjects affected by frontotemporal lobar degeneration using automated longitudinal MRI volumetry," *Hum. Brain Mapp.*, vol. 33, no. 7, pp. 1526–1535, Jul. 2012.

[36] K. Van Leemput, F. Maes, D. Vandermeulen, and P. Suetens, "Automated model-based tissue classification of MR images of the brain," *Med. Imaging Ieee Trans.*, vol. 18, no. 10, pp. 897–908, Oct. 1999.

[37] L. Liang, K. Rehm, R. P. Woods, and D. A. Rottenberg, "Automatic segmentation of left and right cerebral hemispheres from MRI brain volumes using the graph cuts algorithm," *NeuroImage*, vol. 34, no. 3, pp. 1160–1170, Feb. 2007.

[38] L. Liang, K. Rehm, R. P. Woods, and D. A. Rottenberg, "Automatic segmentation of left and right cerebral hemispheres from MRI brain volumes using the graph cuts algorithm," *NeuroImage*, vol. 34, no. 3, pp. 1168–1169, Feb. 2007.
[39] G. Karas, P. Scheltens, S. Rombouts, and et al., "Global and local gray matter loss in mild cognitive impairment and Alzheimer's disease.," *NeuroImage*, no. 23, pp. 708–716, 2004.
[40] K. Chen, E. M. Reiman, G. E. Alexander, D. Bandy, R. Renaut, W. R. Crum, N. C. Fox, and M. N. Rossor, "An automated algorithm for the computation of brain volume change from sequential MRIs using an iterative principal component analysis and its evaluation for the assessment of whole-brain atrophy rates in patients with probable Alzheimer's disease," *NeuroImage*, vol. 22, no. 1, pp. 134–143, May 2004.
[41] S. . Smith, "Fast robust automated brain extraction," *Hum. Brain Mapp.*, vol. 17, no. 3, pp. 143–155, 2002.
[42] J. Ashburner and K. Friston, "Voxel-based morphometry—the methods.," *NeuroImage*, vol. 11, pp. 805–821, 2000.
[43] C. Davatzikos,, A. Genc, D. Xu, and S. . Resnick, "Voxel-based morphometry using the RAVENS maps: methods and validation using simulated longitudinal atrophy.," *NeuroImage*, vol. 14, pp. 1361–1369, 2001.
[44] P. Thompson, K. . Hayashi, G. de Zubicaray,, A. . Janke, S. . Rose, J. Semple, D. Herman, M. . Hong, S. . Dittmer, D. M. Doddrell, and A. . Toga, "Dynamics of gray matter loss in Alzheimer's disease.," *J Neurosci*, vol. 23, pp. 994–1005, 2003.
[45] J. Ashburner, "GM volume," *SPM email list*. Apr-2002.
[46] suz prejawa, "VBM."
[47] M. L. Seghier, A. Ramlackhansingh, J. Crinion, A. P. Leff, and C. J. Price, "Lesion identification using unified segmentation-normalisation models and fuzzy clustering," *NeuroImage*, vol. 41, no. 4, pp. 1253–1266, Jul. 2008.
[48] H. P. Op de Beeck, "Against hyperacuity in brain reading: Spatial smoothing does not hurt multivariate fMRI analyses?," *NeuroImage*, vol. 49, no. 3, pp. 1943–1948, Feb. 2010.
[49] K. J. Fritson, A. . Holmes, K. J. Worsley, J.-B. Poline, C. D. Frith, and R. S. J. Frackowiak, "Statistical parametric maps in functional imaging: A general linear approach," *Hum. Brain Mapp.*, vol. 2, pp. 189–210, 1995.
[50] J. L. Whitwell, "VBMAnAutomatedTechniqueForAssessingStructuralChangesInTheBrain.pdf," *Jounal Neurosci.*, vol. 29, no. 31, pp. 9661–9664, Aug. 2009.
[51] A. Peinemann, S. Schuller, C. Pohl, T. Jahn, A. Weindl, and J. Kassubek, "Executive dysfunction in early stages of Huntington's disease is associated with striatal and insular atrophy: A neuropsychological and voxel-based morphometric study," *J. Neurol. Sci.*, vol. 239, no. 1, pp. 11–19, Dec. 2005.

[52] S. R. Vantaram, “Survey of contemporary trends in color image segmentation,” *J. Electron. Imaging*, vol. 21, no. 4, p. 040901, Oct. 2012.
[53] Y. Ge, R. I. Grossman, J. S. Babb, M. L. Rabin, L. J. Mannon, and D. L. Kolson, “Age-Related Total Gray Matter and White Matter Changes in Normal Adult Brain. Part I: Volumetric MR Imaging Analysis,” *Am. J. Neuroradiol.*, vol. 23, no. 8, pp. 1327–1333, 2002.
[54] C. D. Good, I. S. Johnsrude, J. Ashburner, R. N. A. Henson, K. J. Fristen, and R. S. J. Frackowiak, “A voxel-based morphometric study of ageing in 465 normal adult human brains,” *Biomed. Imaging 2002 5th Ieee Embs Int. Summer Sch.*, p. 16 pp., 15.
[55] C. Pernet, J. Andersson, and Paulesu, “When All Hypotheses are Right: A Multifocal Account of Dyslexia,” *Hum. Brain Mapp.*, vol. 30, pp. 2278–2292, 2009.
[56] Jianbo Shi and J. Malik, “Normalized cuts and image segmentation,” *Pattern Anal. Mach. Intell. Ieee Trans.*, vol. 22, no. 8, pp. 888–905, Aug. 2000.
[57] Z. Wu and R. Leahy, “An optimal graph theoretic approach to data clustering: theory and its application to image segmentation,” *Pattern Anal. Mach. Intell. Ieee Trans.*, vol. 15, no. 11, pp. 1101–1113, Nov. 1993.
[58] J. Malik, S. Belongie, T. Leung, and J. Shi, “Contour and Texture Analysis for Image Segmentation,” *Int. J. Comput. Vis.*, vol. 43, no. 1, pp. 7–27, 2001.
[59] S. Sarkar and P. Soundararajan, “Supervised learning of large perceptual organization: graph spectral partitioning and learning automata,” *Pattern Anal. Mach. Intell. Ieee Trans.*, vol. 22, no. 5, pp. 504–525, May 2000.
[60] S. Wang and J. M. Siskind, “Image segmentation with ratio cut,” *Pattern Anal. Mach. Intell. Ieee Trans.*, vol. 25, no. 6, pp. 675–690, Jun. 2003.
[61] Y. Boykov and M.-P. Jolly, “Interactive graph cuts for optimal boundary and region segmentation of objects in n-d images,” *Int. Confreence Comput. Vis.*, vol. I, pp. 105–112, 2001.
[62] Y. Boykov, O. Veksler, and R. Zabih, “Fast approximate energy minimization via graph cuts,” *Pattern Anal. Mach. Intell. Ieee Trans.*, vol. 23, no. 11, pp. 1222–1239, Nov. 2001.
[63] yuri boykov, O. Veksler, and R. Zabih, “Efficient Approximate Energy Minimization via Graph Cuts,” *Ieee Tpami*, vol. 20, no. 12, pp. 1222–1239, Nov. 2001.
[64] V. Kolmogorov and R. Zabih, “What Energy Functions can be Minimized via Graph Cuts?,” *Ieee Tpami*, vol. 26, no. 12, pp. 147–159, Feb. 2004.
[65] Y. Boykov and V. Kolmogorov, “An Experimental Comparison of Min-Cut/Max-Flow Algorithms for Energy Minimization in Vision,” *Ieee Tpami*, vol. 26, no. 9, pp. 1124–1137, Sep. 2004.

[66] A. Delong, A. Osokin, H. N. Isack, and Y. Boykov, “Fast Approximate Energy Minimization with Label Costs.,” *CVPR*, Jun. 2010.
[67] Y. Boykov, O. Veksler, and R. Zabih, “Markov Random Fields with Efficient Approximations,” *Ieee Cvpr*, pp. 648–655, 1998.
[68] V. Kwatra, A. Schdl, I. Essa, A. Bobick, and G. Turk, “Graphcut textures: Image and video syntesis using graph cuts,” *Acm Trans. Graph.*, no. Proc. SIGGRAPH, Jul. 2003.
[69] H. Ishikawa and D. Geiger, “Segmentation by grouping junctions,” *Comput. Vis. Pattern Recognit. 1998 Proc. 1998 Ieee Comput. Soc. Conf.*, pp. 125–131, 23.
[70] V. Chen and Su Ruan, “Graph cut segmentation technique for MRI brain tumor extraction,” *Image Process. Theory Tools Appl. Ipta 2010 2nd Int. Conf.*, pp. 284–287, 7.
[71] S. Despotovic, A. Platisa, E. Vansteenkiste, A. Pizurica, K. Deblaere, and W. Philips, “Automatic 3D graph cuts for brain cortex segmentation in patients with focal cortical dysplasia,” *Ieee Cvpr*, 2011.
[72] S. A. Sadananthan, W. Zheng, M. W. L. Chee, and V. Zagorodnov, “Skull stripping using graph cuts,” *NeuroImage*, vol. 49, no. 1, pp. 225–239, Jan. 2010.
[73] R. K.-S. Kwan, A. C. Evans, and G. . pike, “MRI simulation-based evaluation of image-processing and classification methods,” *Ieee Trans. Med. Imaging*, vol. 18, no. 11, pp. 1085–1097, Nov. 1999.
[74] R. K.-S. Kwan, A. C. Evans, and G. . pike, “An Extensible MRI Simulator for Post-Processing Evaluation",” presented at the Visualization in Biomedical Computing, 1996, vol. 1131.
[75] D. . Collins, A. . Zijdenbos, V. Kollokian, J. . Sled, N. J. Kabani, and A. C. Evans, “Design and Construction of a Realistic Digital Brain Phantom,” *Ieee Trans. Med. Imaging*, vol. 17, no. 3, pp. 463–468, Jun. 1998.
[76] M.-E. Algorri and F. Flores-Mangas, “Classification of anatomical structures in MR brain images using fuzzy parameters,” *Biomed. Eng. Ieee Trans.*, vol. 51, no. 9, pp. 1599–1608, 2004.
[77] A. F. Goldszal, C. Davatzikos, D. L. Pham, M. X. Yan, R. N. Bryan, and S. M. Resnick, “An image-processing system for qualitative and quantitative volumetric analysis of brain images,” *J. Comput. Assist. Tomogr.*, vol. 22, no. 5, pp. 827–837, 1998.
[78] C. Xu, D. L. Pham, M. E. Rettmann, D. N. Yu, and J. L. Prince, “Reconstruction of the human cerebral cortex from magnetic resonance images,” *Med. Imaging Ieee Trans.*, vol. 18, no. 6, pp. 467–480, 1999.
[79] “MATLAB - The Language of Technical Computing.” [Online]. Available: http://www.mathworks.com/products/matlab/. [Accessed: 17-Apr-2013].

[80] "BrainSuite." [Online]. Available: http://brainsuite.loni.ucla.edu/. [Accessed: 17-Apr-2013].
[81] "Obama unveils funding for brain mapping project (full speech) - The Washington Post." [Online]. Available: http://www.washingtonpost.com/politics/obama-unveils-funding-for-brain-mapping-project-full-speech/2013/04/02/d5e590dc-9ba2-11e2-9bda-edd1a7fb557d_video.html. [Accessed: 25-Apr-2013].